Implementation of standard testbeds for numerical relativity

M C Babiuc[1], S Husa[2], I Hinder[3], C Lechner[4], E Schnetter[5,6], B Szilágyi[7], Y Zlochower[8], N Dorband[7], D Pollney[7] and J Winicour[7,9]

1 Department of Physics and Physical Science, Marshall University, Huntington, WV 25755, USA
2 Friedrich Schiller University Jena, Max-Wien-Platz 1, 07743 Jena, Germany
3 Center for Gravitational Wave Physics, The Pennsylvania State University, University Park, PA 16802, USA
4 Weierstrass Institute for Applied Analysis and Stochastics (WIAS), Mohrenstraße 39, 10117 Berlin, Germany
5 Center for Computation & Technology, 216 Johnston Hall, Louisiana State University, Baton Rouge, LA 70803, USA
6 Department of Physics and Astronomy, 202 Nicholson Hall, Louisiana State University, Baton Rouge, LA 70803, USA
7 Max-Planck-Institut für Gravitationsphysik (Albert-Einstein-Institut), Am Mühlenberg 1, 14076 Golm, Germany
8 Center for Computational Relativity and Gravitation, School of Mathematical Sciences, Rochester Institute of Technology, 78 Lomb Memorial Drive, Rochester, New York 14623, USA
9 Department of Physics and Astronomy, University of Pittsburgh, Pittsburgh, Pennsylvania 15260, USA

Abstract.

We sharpen our discussion of the design and implementation of the initial round of testbeds for numerical relativity which was presented in the first paper of the Apples with Apples Alliance. We present benchmark results for various codes which provide templates for analyzing the testbeds and to draw conclusions about various features of the codes. This allows us to sharpen the initial test specifications and add theoretical insight.

PACS numbers: 04.70.Bw, 04.25.Dm, 04.40.Nr, 98.80.Cq

1. Introduction

For decades, the field of numerical relativity has been dominated by an often painful quest for stable black-hole inspiral simulations. More than forty years after Hahn and Lindquist's first pioneering numerical simulation of colliding black holes [1], this quest has recently turned into a gold-rush when Pretorius's breakthrough simulation [2] based on a harmonic code was followed by simultaneous invention of the "moving punctures" method by two independent groups [3, 4].

The primary motivation for solving the binary black hole problem in numerical relativity has however been to supply waveforms for gravitational wave detectors. This goal demands an approach that goes beyond the efforts that have lead to an explosion in publications from the binary black hole community. Cross-validation of

waveforms between different groups (and codes) and comparison with post-Newtonian predictions will be essential for numerical waveforms to be used in the computationally expensive searches conducted by the international gravitational wave community. The importance of cross-validation of numerical relativity results as a community effort was foreseen by the Apples with Apples Alliance (AwA) [5], which has presented a first round of standardized testbeds [6]. This first round comprises four tests with periodic boundaries, designed to efficiently exhibit code instability and inaccuracy. Instabilities currently receive less attention, since it has turned out that, paradoxically, binary black hole evolutions are in some sense a simpler problem than had been expected, and current codes evolving binary black holes do not typically show instabilities. The same codes *will* however have difficulties with some of the testbeds presented in the first round. The theoretical understanding of what works and what does not in numerical relativity is still very much an open problem. One crucial theoretical advance, which has been made since the publication of our first paper [6], is the development of a theory for well-posed second order in space, first order in time systems [7, 8, 9, 10, 11, 12, 13], which has been extended to a basic understanding of numerical stability for such systems [11, 12, 13].

Over the past years several groups have committed their test results to a publicly available data repository, with activities being coordinated via the website `http://www.ApplesWithApples.org`. The purpose of the present paper is to document these developments and discuss their feedback with respect to code performance, to test improvement and to the design of further tests. While predating the binary black hole breakthroughs, we believe that the initial Apples with Apples tests and results are still valuable as providing a first testbed for a community effort in numerical relativity.

The tests side-step many issues that would arise in a precise discussion of the binary black hole problem, such as the issue of boundaries. We make the natural choice of periodic boundaries for a first round of tests to isolate the performance of evolution algorithms. This is equivalent to evolution on the topology of a 3-torus in the absence of boundaries. However, in the context of general relativity, this introduces complications of a cosmological nature regarding the instability of Minkowski spacetime to perturbations on a compact manifold, as has been discussed in [6].

Establishing a paradigm for standardized testbeds for numerical relativity is a formidable task in itself. We can draw on experience from other fields, such as computational hydrodynamics where such testbeds have been used for a long time (for an overview of CFD testbed resources on the web, see e.g. [14]; for an example of initial value ordinary differential equation (ODE) test-suites see [15]). However, general relativity comes with its own issues that introduce extra complications. First of all, it is important to realize that the numerical relativity community is small, with very limited available manpower. In contrast to the size of the field, we are trying to solve many difficult problems at the same time. Numerical methods are being developed in parallel with the formulation of the continuum problem, with the construction of physically relevant initial data sets and with the unraveling of the physical processes involved in the systems under investigation. All of this is, so far, without the help of comparison with experiments. Groups working in the field are faced with many fundamental questions in designing their approaches. Codes are in a state of flux that makes careful documentation easy to postpone. A good example is the issue of boundaries, which can be taken to be either a cubic grid boundary or

a smooth spherical boundary, which can either be mapped to infinity or given some finite artificial location, and which are further complicated by gauge freedom and the requirements of constraint preservation. Useful comparison of the wide variety of resulting codes requires simple tests which isolate an important facet of the problem.

We distinguish two fundamentally different types of testbed: The first type compares different codes and methods in the treatment of a physically interesting set of solutions. In the context of the binary black hole problem, a detailed comparison of nonspinning equal-mass inspiral would be a natural example. The second type are idealized situations, such as the "shock tube test" [16] in computational fluid dynamics. This is the type of testbed we discuss in the present paper, where we restrict ourselves to a greatly simplified first set of tests [6]: periodic grids and strict test specifications, which as far as practicable define all the details of a simulation except the formulation of the Einstein equations. Our experience with the first round of testbeds confirms this decision: even the analysis of these simple situations has proved quite challenging. Our conclusions in Sec. 7 discuss how the experience from the present round of tests can be used in our development of black hole tests.

We identify five main aims of standardized tests of the "idealized" type:

(i) Standardized tests should provide the young and fast-changing community of numerical relativists with a common reference frame which will help integrate different efforts to produce a coherent picture of what works and what does not, and thus reduce the dependence on anecdote and fashion.

(ii) Tests should be efficient in revealing instabilities or other weaknesses of an algorithm, both regarding simplicity of the analysis, run time and implementation.

(iii) Tests should help identify where problems come from, as a step toward improvement of the algorithms.

(iv) Tests should facilitate comparisons between approaches regarding different continuum formulations, spatial discretizations, time integrators, uses of artificial dissipation, etc.

(v) The development of testbeds should eventually lead to useful code comparisons for judging the validity of physically interesting simulations, e.g. the binary black hole problem.

Point (i) has been addressed by organizing this project as a community initiative, which seeks broad participation and provides test results via web pages and a CVS repository [5]. Regarding point (ii), in this paper we review our original test specifications and propose modifications to promote efficiency. Point (iii) is essential for the character of this paper: we focus on presenting test results as a template for analyzing and interpreting results, rather than just presenting the broadest possible listing of test output for a maximal number of codes. We feel that it is essential to stress this point: tests which do not directly correspond to a physically interesting situation are only valuable if they improve our understanding of what really goes on with a certain code. Only then can we hope to carry over test benefits to other situations. Such analysis does of course require a certain effort.

Point (iv) is dealt with by providing "standard candle results" in the CVS repository, i.e., benchmarks that have been obtained with very strictly defined specifications. Point (v) represents the ultimate goal of the AwA Alliance.

The code descriptions and test data on which this paper is based are described in Sec. 2. The results for the four standardized tests are discussed in Secs. 3, 4,

5 and 6. Conclusions from the test results and our experiences with the testing procedures, along with recommendations for changes in the standard test specifications and proposals for new tests, are given in Sec. 7.

The plots presented in this paper are based upon test output in the CVS repository. Many of these tests were run with codes in which artificial dissipation was only introduced implicitly through the use an iterated Crank-Nicholson (ICN) time integrator. It had been a naive hope at the beginning of this project that the use of ICN might provide a way to standardize the introduction of dissipation. Most numerical relativity groups now use Runge-Kutta time integrators with the explicit addition of Kreiss-Oliger dissipation (see Appendix B.2). It has been found that many of the test results presented here could be greatly improved by such explicit use of dissipation. In addition to artificial dissipation, most codes used to simulate binary black holes use higher order approximations than the second order accurate codes being compared here. Consequently, we want to emphasize that the results exhibited in this paper should not be used to make judgments on particular approaches, but that our purpose is to assess and improve the test suite and to provide a basis for future code comparisons.

2. Code descriptions

In order to ensure a consistent presentation of test output, we present a brief account of the numerical codes and algorithms which have been used to produce the data on which this paper is based. All data are publicly available via the CVS repository (see [5] for details). The four standardized tests are denoted by ROBUST (the Robust Stability Test), LINEAR (the Linear Wave Test), GAUGE (the Gauge Wave Test) and GOWDY (the Gowdy Wave Test). Table 1 summarizes the output data that have been submitted for the various codes.

CODE	ROBUST	LINEAR	GAUGE	GOWDY
Abigel_harm	++	++	++	++
AEI_CactusEinsteinADM	+	−−	−−	++
Kranc_FreeADM	+	+	+	+
CCATIE_BSSN	++	++	++	++
Kranc_BSSN	++	++	++	++
LazEv_BSSN	++	++	++	++
HarmNaive	++	++	++	++
KrancNOR	++	++	++	++
KrancFN	++	++	++	−−
LSU_HyperGR	++	++	++	++

Table 1. Test output and codes considered in this article. The code abbreviations are explained below, along with a description of the finite difference algorithm. A "++" indicates a full complement of test output in the CVS, a "+ indicates partial output which has been used for our analysis, a "−" indicates partial output on which no meaningful conclusions could be drawn and a "−−" indicates no output.

The usefulness of this data depends upon good code documentation. It is beyond the scope of this paper to provide such documentation for all the codes involved. However, we will outline some basic code information which is necessary to interpret

the test results. The complexity of this task is somewhat alleviated because all the codes represented here follow a method of lines approach. We will organize the code descriptions along the following guidelines.

- A description of the *continuum formulation*, including a list of all variables, their associated evolution equations and constraints (both differential and algebraic), equations governing the lapse and shift and a specification of any free parameters. Terms and differential operators in the equations should be ordered in the way that they are approximated by finite difference expressions in order to avoid ambiguities associated with the Leibniz rule. The hyperbolicity classification should be provided, if known.
- A description of the *semi-discrete system*, describing the spatial finite difference equations on each time level, including the rules for discretizing partial derivatives as centered or one-sided finite differences and any other discretization techniques, such as spatial averaging or dissipation. For complicated systems, the finite difference rules may be specified only for the principal part, with further details supplied by references. (Here we provide some basic reference material in Appendix A and Appendix B for compactness of presentation.)
- A description of the *numerical time update scheme*. All manipulations of data between intermediate time steps should be specified, such as enforcing a constraint.

As an example, we consider two inequivalent algorithms for the wave equation $\Box\phi = 0$ (with unit lapse, zero shift and spatial metric γ_{ij}), which should be expected to result in different code performance. In both cases the second order in time system is reduced to first order in time by introducing the variable $\pi = \partial_t\phi$, and applying, say, 4th order Runge-Kutta (see Appendix B) to the ODEs of the semi-discrete system obtained using the method of lines. Two different codes can based upon the following descriptions.

Description **I**:

(i) The continuum system is

$$\partial_t\phi = \pi, \tag{1}$$

$$\partial_t\pi = \frac{1}{\sqrt{\gamma}}\partial_i(\sqrt{\gamma}\gamma^{ij}\partial_j\phi). \tag{2}$$

(ii) The semi-discrete version is obtained by replacing all partial derivatives in (2) by centered differences:

$$\partial_t\pi = \frac{1}{\sqrt{\gamma}}D_{0i}(\sqrt{\gamma}\gamma^{ij}D_{0j}\phi),$$

where D_{0i} is the centered difference operator D_0 applied in direction i (see Appendix B.1).

Description **II** (inequivalent with **I**):

(i) The continuum system is

$$\partial_t\phi = \pi, \tag{3}$$

$$\partial_t\pi = \gamma^{ij}\partial_i\partial_j\phi + \frac{1}{\sqrt{\gamma}}\partial_i(\sqrt{\gamma}\gamma^{ij})\partial_j\phi. \tag{4}$$

(ii) The semi-discrete version is obtained by replacing the partial derivatives in (2) by centered differences according to

$$\begin{aligned}&\gamma^{ij}\partial_i\partial_j\phi + \frac{1}{\sqrt{\gamma}}\partial_i(\sqrt{\gamma}\gamma^{ij})\partial_j\phi \\ &= \gamma^{ij}D_{+i}D_{-j}\phi + \frac{1}{\sqrt{\gamma}}D_{0i}(\sqrt{\gamma}\gamma^{ij})D_{0j}\phi \end{aligned} \tag{5}$$

where D_{+i} and D_{-i} represent forward and backward centered finite differences in the respective directions (see Appendix B.1).

The codes resulting from these two descriptions produce substantially different performance because of the "checkerboard" design of the stencil used in **I**. Descriptions of the specific codes used in this paper are given in Appendix A.

3. Robust stability test

The robust stability test was intended as a first screen to eliminate many unstable evolution algorithms. The particular importance of this test was due to the fact that instabilities of numerical codes appeared as a prime obstacle to "solve" the binary black hole problem, and essentially no theoretical understanding was available to discuss the well-posedness and numerical stability of first order in time, second order in space formulations of the Einstein equations, which have been and still are popular in the field. Recently, a theoretical framework has become available to discuss the well-posedness and numerical stability of such mixed order formulations of the Einstein equations [17, 7, 8, 9, 10, 18, 11, 12, 13], and it has been extended to the problem of discretizing the equations in the context of the method of lines [11, 12, 13]. As a consequence of both the recent breakthroughs in the binary black hole problem and the theoretical advances, numerical stability has become a *relatively* minor issue in practice (although there certainly remain interesting mathematical questions to be pursued). We thus restrict ourselves to a minimal discussion here, as is sufficient to understand the data available in our test results repository. For a more in-depth discussion of theoretical and practical aspects of numerical stability and the robust stability test we refer to [11], which has been directly motivated by numerical results obtained within this project.

While the other tests give quantitative information about an evolution system, e.g. the magnitude of the numerical error, the result of the robust stability test is "pass" or "fail". A stable numerical algorithm is only possible if the underlying continuum problem is well-posed [19]. In the well-posed case an instability might still arise, either from the numerical technique or from the existence of an exponential mode in the continuum problem. The test is designed to avoid continuum instabilities by considering small perturbations of the Minkowski metric. In addition to providing efficient detection of unstable numerical algorithms (or coding errors) affecting the principal part of the evolution system, it is also intended to spot instabilities arising from ill-posed systems, such as weakly hyperbolic systems.

As an example, consider the weakly hyperbolic system

$$\begin{aligned} u_{,t} &= u_{,x} + v_{,x} \\ v_{,t} &= v_{,x} \end{aligned} \tag{6}$$

with the periodic solutions

$$u = \omega t \cos\omega(t+x)\,, \quad v = \sin\omega(t+x) \tag{7}$$

$$\omega = 2\pi m\,, \quad m = 1, 2, 3, ...$$

on the domain $-.5 \leq x \leq .5$. In terms of the L_2 norm

$$N = \left(\int_{-.5}^{.5} (u^2 + v^2) dx \right)^{1/2}, \tag{8}$$

the Cauchy data for (7) at $t = 0$,

$$u = 0\,, \quad v = \sin \omega x, \tag{9}$$

has norm $N(0) = 1/\sqrt{2}$. However, because of (7), $N(t) \sim \omega t$ for large ω. This leads to a violation of the well-posedness requirement that in any finite time interval

$$N(t) < Ae^{Kt} N(0), \tag{10}$$

in terms of constants A and K independent of the Cauchy data.

For discretized systems we can not test well-posedness directly, but rather we test the analogous concept of numerical stability, i.e., we aim at establishing the existence of constants A and K, which give rise to the bound

$$\frac{\|v^n\|}{\|v^0\|} \leq Ae^{Kt_n}, \tag{11}$$

where v^n is the solution of the discrete system at time $t_n = nk$. The test is passed if such a bound can be established, and is failed otherwise. In the discretized version of a weakly hyperbolic problem, with grid displacement h, the perturbation of a simulation by random initial data can be expected to excite numerical error which grows linearly in time according to $u \sim t/h$, corresponding to the shortest wave number $\omega \sim 1/h$. This would then lead to secular error growth which increases with resolution. Although the system (6) is well-posed with respect to a stronger norm including a $v_{,x}^2$ term, a generic perturbation of (6) by lower order terms would nevertheless produce an exponentially growing instability which cannot be bounded. See [20] for a more general discussion of such weakly hyperbolic systems.

The key idea of setting initial data for this test is to distribute energy roughly equally over all frequencies. This is a particularly efficient way to reveal growing modes if the growth rate increases with resolution, as is the case if the discretization is unstable or if the continuum problem is ill-posed. In our test we use a spectrum generated by random initial data.

The robust stability test as formulated here tests numerical stability in the linear, constant coefficient regime. This not only simplifies the formulation and execution of the test but it also provides better insight into both the continuum and discrete problems. In particular, for most formalisms it is possible to construct explicit solutions to the discrete equations in this regime and to obtain very precise insight.

In spite of its simplicity, the robust stability test exhibits various subtle difficulties in designing a single test prescription that is universally effective for all evolution systems and numerical methods. Some particular problems are:

- For random initial data, where a significant part of the total energy is in high frequencies, dissipation has a large effect. Some intrinsic dissipation is unavoidable in finite difference evolution algorithms, and adding artificial dissipation may be necessary to stabilize certain algorithms [11], and insufficient to stabilize others (such as algorithms for weakly hyperbolic systems). Simulations of variable coefficient, nonlinear systems normally require numerical dissipation to obtain a stable evolution, e.g. by adding Kreiss-Oliger type

dissipation [20] (see Appendix B.2). Dissipation can however increase the time scale on which instabilities become apparent. The detailed way dissipation affects instabilities varies with the spatial discretization (we only consider second order approximations here), with the time integrator, with the grid resolution and with the Courant number.

- As discussed in the above example, well-posedness and numerical stability are defined with respect to a certain norm. Using an inappropriate norm can yield misleading results. Second order systems require different norms than first order systems [11].
- Numerical stability of an explicit time integration algorithm can only be expected if the time step is appropriately restricted by a Courant-Friedrichs-Lewy (CFL) condition. It is important to distinguish between resolution dependent blowup associated with ill-posedness from blowup resulting from a CFL violation. For sufficiently complicated 3D algorithms, the CFL limit might not be readily deduced from analytic arguments. As an example, exponential growth of the ADM algorithm was mistakenly provided as an illustration of a failed robust stability test in [6] . It took subsequent testing and analysis to reveal that this exponential growth resulted from a CFL violation and that otherwise the weakly hyperbolic instability of ADM resulted in a secular (linear in time) growth.

As a result of such considerations, we will not try to present a single universally applicable specification for the robust stability test. Instead, while keeping the original spirit of the test as a simple and useful first screen, we propose some changes in the guidelines, as discussed below.

An important issue when performing stability tests is whether the high frequency modes are damped. This has important bearing on the long-time behavior of the robust stability test: all damped modes will decay in time; eventually the undamped frequencies of the discrete system will dominate the signal. If an analysis of damping factors has not been performed, the test can therefore also be useful in detecting the spectrum of frequencies which are not damped. It has been pointed out in [11] for standard discretizations of first order in space systems that the "checkerboard" mode is undamped, while for typical second order systems it is damped. Since the "checkerboard" mode is not realized on grids with an odd number of points, we adopt the practice of always using an even number of grid points so as not to muzzle a potential instability.

In our original specifications, we proposed the relatively large time step $dt = 0.5dx$, which turned out to be larger than the CFL limit for the ADM system. Since a smaller dt also decreases the amount of dissipation inherent in a time integrator, we now propose a relatively small time step to avoid distortion of results due to dissipation. Common time integrators in current practice in numerical relativity are ICN, RK3 and RK4 (sorted by decreasing internal amount of dissipation). A sufficiently small time step would yield similar results for all of them. We therefore propose to run with $dt = 0.1dx$, which can be further reduced in case of doubt. We also drop the original restriction to a particular numerical integrator.

The robust stability test is based upon a small perturbation of Minkowski space, with random numbers at each grid point prescribed as initial data for every evolution variable. For example, the 3-metric is initialized as $\gamma_{ij} = \delta_{ij} + \epsilon_{ij}$, where the ϵ_{ij} are independent random numbers. For systems that use variables which correspond to spatial derivatives of the ADM 3-metric and extrinsic curvature, an ambiguity arises:

noise can be added uniformly to all variables, or to the ADM initial data before taking derivatives. There are similar ambiguities in second order systems regarding how the range of the random numbers should scale with resolution. For uniformity of description, we propose to do the simplest thing, namely to apply noise to all evolution variables in the same way. We propose the range of $\pm 10^{-10}$ for all variables, the same range used for the lowest resolution in the original specifications.

Following common practice at the time, the Hamiltonian constraint was used to analyze test results. Again following [11], we now propose a pass/fail analysis based upon whether the time behavior of the norm satisfies (11).

Instabilities caused by the ill-posedness of the evolution system, or by coding errors in treating the principal part, are already apparent in one-dimensional tests, which can be performed quickly and economically. Some testing of 3-dimensional modes is also desirable. Our core test specification combines both 1D and 3D features by running in a thin channel with the specifications:

- Simulation domain: $x \in [-0.5, +0.5]$
- Grid: $x_n = -0.5 + (n - \frac{1}{2})dx, \quad n = 1 \ldots 50\rho, \quad dx = dy = dz = 1/(50\rho), \quad \rho = 1, 2, 4, \ldots$
- Time step: $dt = dx/10 = 0.002/\rho$

The use of 4 distinct gridpoints in the y and z directions allows for the checkerboard mode (ghost points may be necessary depending upon the numerical scheme). The generalization to full cube 3D tests is straightforward, and may add further clarification in case of dubious results.

The test should be run until one is confident that dissipation effects do not cloud the result. Without artificial dissipation, a runtime of one crossing time, using output at every time step, is usually sufficient. This corresponds to 500ρ time steps. The test is passed if the norm satisfies the inequality (11) for all resolutions, for a fixed choice of A and K, The norms for both first and second order systems recommended in [11] are publicly available as Cactus thorns [21]. An example of how this analysis works is given in Fig. 1. The Abigel_harm code, which is based upon a symmetric hyperbolic formulation, passes the test; whereas the HarmNaive code, which is based upon a weakly hyperbolic formulation, fails the test.

4. Linearized wave test

A prime physical objective of numerical relativity is to compute the waveform from a system of black holes and neutron stars. This test checks the ability of a code to propagate a linearized gravitational wave, which is a minimally necessary attribute for reliable wave extraction from strong sources. For the choice of unit lapse and vanishing shift, the linearized wave is given by the metric

$$ds^2 = -dt^2 + dx^2 + \left(1 + A\sin(\frac{2\pi(x-t)}{d})\right) dy^2 + \left(1 - A\sin(\frac{2\pi(x-t)}{d})\right) dz^2, \quad (12)$$

with the wave amplitude $A = 10^{-8}$ which is small enough for quadratic terms to be lost in numerical roundoff. This describes a plane wave traveling in the x-direction The evolution domain is matched to the wavelength $d = 1$ so that the resulting periodicity and toroidal topology avoids dealing with nontrivial boundary conditions. A rotation of the propagation direction to the diagonal in the (x, y) plane can be used to test 2D features. Setting $d' = d\sqrt{2}$ retains periodicity along those directions.

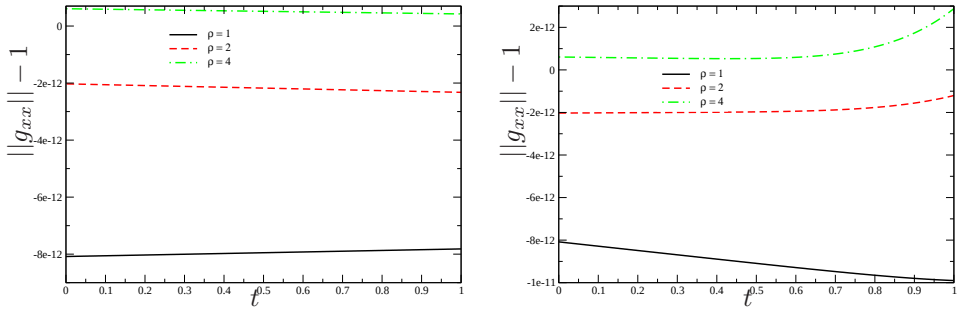

Figure 1. Convergence results for the robust stability test with the Abigel_harm (left) and HarmNaive (right) codes, for runs of 1 crossing time. The graphs show the L_2 norm of the error in g_{xx}, as a function of time, and shifted by -1. As seen from the slopes of the graphs, the Abigel_harm code (left) passes the test, because there is no increasing rate of error growth with higher resolution, while the HarmNaive code (right) fails the test because the growth rate increases with resolution.

The grid is set up as follows:

- Simulation domain:

$$\begin{array}{rllll} \text{1D:} & x \in [-0.5; +0.5], & y = 0, & z = 0, & d = 1 \\ \text{diagonal:} & x \in [-0.5; +0.5], & y \in [-0.5; +0.5], & z = 0, & d' = \sqrt{2} \end{array}$$

- Grid: $x^i = -0.5 + (n - \frac{1}{2})dx, \quad n = 1 \ldots 50\rho, \quad dx = 1/(50\rho), \quad \rho = (1, 2, 4)$
- Time step: $dt = dx/4 = 0.005/\rho$.

The 1D tests are run for $T = 1000$ crossing times and the 2D diagonal tests for $T = 100$ in order to save computational resources.

The test checks the accuracy of the code in propagating both the amplitude and phase of the wave. It can reveal whether excessive dissipation has been necessary for good long term performance in the robust stability test. For the $\rho = 1$ coarsest grid ($N = 50$ grid zones), there is not enough resolution for second order accurate codes to obtain accurate phase propagation and the corresponding runs should only be viewed as an economical first check on the code. The most useful comparisons are with the $\rho = 4$ grid.

Fig. 2 compares snapshots of the 1D wave after 1000 crossing times which were obtained with a variety of codes using the $\rho = 4$ finest grid. For reference, the exact waveform is also plotted. The snapshots for three of the codes, Abigel_harm, HarmNaive and LazEv_BSSN, are very similar and provide a good benchmark for the accuracy that can be achieved at this resolution. They very closely match the exact solution in amplitude but show a phase delay, similar to the delay seen in the following gauge wave test. It should be expected that phase accuracy could be improved by going to fourth order accurate methods. The good accuracy of the HarmNaive code illustrates that instabilities associated with a weakly hyperbolic system are not necessarily evident in linearized tests where, as discussed in Sec. 3, the unstable modes only grow secularly in time. The KrancFN code gives good accuracy for the amplitude but a much larger error in phase. The CCATIE code shows poor accuracy in both phase and error. It is beyond the scope of this paper to explain the discrepancy between the performance of the two BSSN codes.

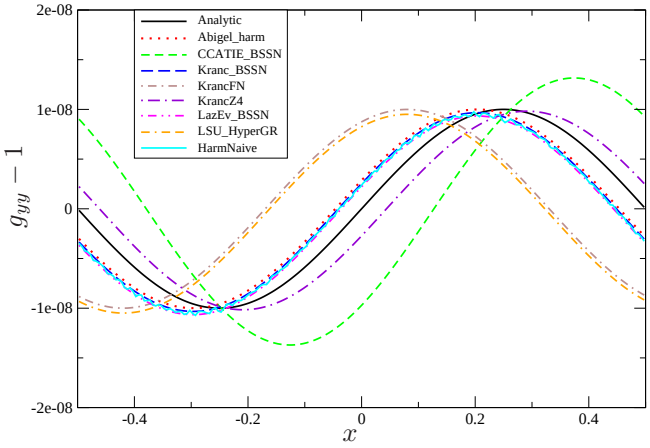

Figure 2. Comparison snapshots of $g_{yy}(x) - 1$ at $t = 1000$ for the 1D linearized wave test.

The 1D linear wave test is simple and economical to perform. Although the test is not very demanding, the results for the metric component g_{yy} in Fig. 2 show that it provides a benchmark which can be useful to identify weaknesses in code performance. The 2D tests require more computer time and the results were typically in line with expectations from the 1D results.

5. Gauge wave test

The gauge wave test is based on a nonlinear gauge transformation of Minkowski spacetime. Although the correct solution is a flat spacetime, nonlinear effects and the nontrivial geometry of the time slices can easily trigger continuum instabilities in the equations. For simple examples of such effects see [22] for a nonlinear wave equation on flat space, designed to model problems arising in this testbed, and [23] for a linear example of how nontrivial geometry of the slicing can trigger instabilities already for the Maxwell equations.

The one-dimensional testbed is defined by the 4-metric

$$ds^2 = -H dt^2 + H dx^2 + dy^2 + dz^2, \tag{13}$$

where

$$H = H(x - t) = 1 - A \sin\left(\frac{2\pi(x - t)}{d}\right), \tag{14}$$

which describes a sinusoidal gauge wave of amplitude A propagating along the x-axis. The grid layout and time step are chosen as for the linear waves test in Sec. 4, and a rotation of axes again gives rise to a 2D version.

While the gauge wave metric has a rather simple form, the test proved to be challenging for most evolution codes. One anticipated source of growing error is the instability of a flat space with T^3 topology [6]. Another problem is the existence of a family of harmonic, exponential gauge modes corresponding to $H \to e^{\lambda t} H$ (for arbitrary λ) [22]. The testbed itself corresponds to $\lambda = 0$, but numerical error can easily excite modes that result in either exponentially increasing or decaying metric

components. Additional instabilities may be present in individual systems, depending on the detailed form of the reduced evolution system for the particular formulation. Many such instabilities can be identified by looking at the growth of the constraints for the formulation. In addition to instabilities that correspond to solutions of the continuum problem, individual codes may suffer from numerical instabilities depending on the discretization schemes. These would typically be seen as high frequency modes and, for well-posed systems, can be cured by adding artificial dissipation to the numerical algorithm.

Our original specifications [6] were to run the the test with amplitudes $A = 0.01, 0.1$. Many codes have been sufficiently improved to handle larger amplitudes, which is generally more efficient in detecting instabilities with smaller run times. Accordingly, we recommend performing this test with an amplitude of $A = 0.5$. Note that so far no BSSN code has demonstrated satisfactory performance for this test, and for brevity we do not include BSSN results here.

5.1. Results

5.1.1. Results for the Abigel_harm Code For this particular testbed most components of the densitized metric $\bar{g}^{\mu\nu} = \sqrt{-g}g^{\mu\nu}$ have trivial values, the non-trivial ones being

$$\bar{g}^{yy} = \bar{g}^{zz} = H \tag{15}$$

The original implementation of the Abigel code based upon (A.9) leads to a numerically stable and convergent code, with no high frequency modes generated. However, as shown by the dramatic growth of the rescaled error plotted in Fig 3, the gauge wave excites exponential modes $\bar{g}^{yy} = \bar{g}^{zz} = e^{\lambda t}H$, $\lambda > 0$. This can be understood in terms of solutions of the harmonic system whose densitized metric components are all trivial except for

$$\bar{g}^{yy} = \bar{g}^{zz} = F(t, x). \tag{16}$$

The resulting source term $S^{\mu\nu}$ in Eq. (A.9) vanishes except for the components

$$S^{yy} = S^{zz} = \frac{-F_t^2 + F_x^2}{F}. \tag{17}$$

The PDE for $F(t, x)$, which results from inserting (16) - (16) into Eq. (A.9), reduces to $(-\partial_t^2 + \partial_x^2) \log F = 0$, which admits the exponential solutions $F = e^{\lambda t}H$. These solutions satisfy the harmonic constraints and the reduced harmonic system Eq. (A.9), so that they are also solutions of the full Einstein equations. Therefore all codes using harmonic gauge conditions might be expected to excite this mode.

In the case of the Abigel_harm code, these modes were suppressed by building semi-discrete conservation laws into the code which, for the gauge wave initial data, would not be obeyed by the exponential solution. Namely, by writing (A.9) in the flux-conservative form (A.10), the principle part of the resulting equation has vanishing source term, $\tilde{S}^{\mu\nu} = 0$, for this test. A summation by parts numerical algorithm then gives rise to the semi-discrete conservation law

$$\partial_t \sum_{I,J,K} \left(g^{t\beta} \partial_\beta \bar{g}^{\mu\nu} \right) = 0. \tag{18}$$

While this is a non-generic result (most space-times would give a non-zero source term), building this conservation law into the principal part of the system has proved effective not only in this particular case but in the other Apples with Apples tests considered in this paper, as well as in further proposed tests [22, 24, 25].

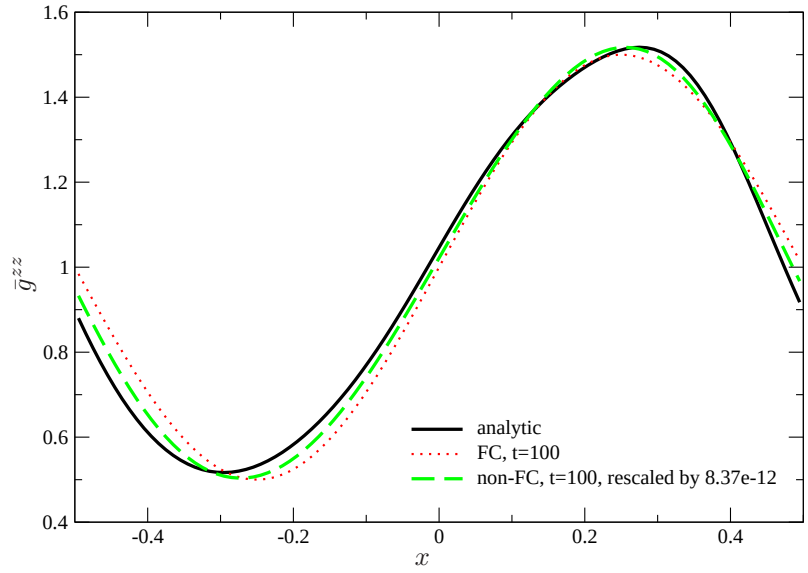

Figure 3. Comparison of code performance between the non-flux-conservative (non-FC) and flux-conservative (FC) versions of the Abigel_harm code, showing graphs of $\bar{g}^{zz}(x)$ at $t = 100$ for a gauge wave of amplitude $A = 0.5$ on the $\rho = 2$ grid. In the non-FC case the graph is rescaled by the average of the plotted function, showing $\bar{g}^{zz}/avg(\bar{g}^{zz}) \approx \bar{g}^{zz}/\exp(29.8)$. The good overlap of this rescaled function with the analytic value clearly indicates that the dominant error of the non-FC code is a multiplicative function of t. Measurements at $t = 100$ for the non-FC code show that logarithm of the spatial average of $\bar{g}^{zz}$ scales roughly as $(dx)^2$, i.e., $\log(avg(\bar{g}^{zz})_{\rho=1}) \approx 110.8, \log(avg(\bar{g}^{zz})_{\rho=2}) \approx 29.8, \log(avg(\bar{g}^{zz})_{\rho=4}) \approx 7.52$, suggesting that the multiplicative error has exponential growth of the form $\exp(O((dx)^2) \cdot t)$.

As shown in Figs. 4 - 6, the flux-conservative code does not develop exponential error modes – the main source of error is phase error, when running with the original ICN integrator (see [24] for results with RK4.) In order to further illustrate this point, Figs. (4 - 6) give test results for both the 1D and 2D versions with amplitudes of $A = 0.01,\ 0.1,\ 0.5$,

5.1.2. Results for the HarmNaive System This naive harmonic system, although weakly hyperbolic, behaves identical to the symmetric hyperbolic Abigel_harm code for this testbed. This can be understood given that the RHS for the mixed space-time components of the evolution system vanish, i.e.

$$\partial_t \bar{g}^{it} = -\partial_j \bar{g}^{ij} = 0, \tag{19}$$

which implies that the time-time component of the RHS also vanishes, i.e.,

$$\partial_t \bar{g}^{tt} = -\partial_j \bar{g}^{tj} = 0. \tag{20}$$

The test-results confirm this.

As expected, tests for the ADM-system also behave identically, since the naive harmonic system can be understood as a formulation of the ADM-system in the harmonic gauge. We therefore skip a separate discussion of the ADM-system.

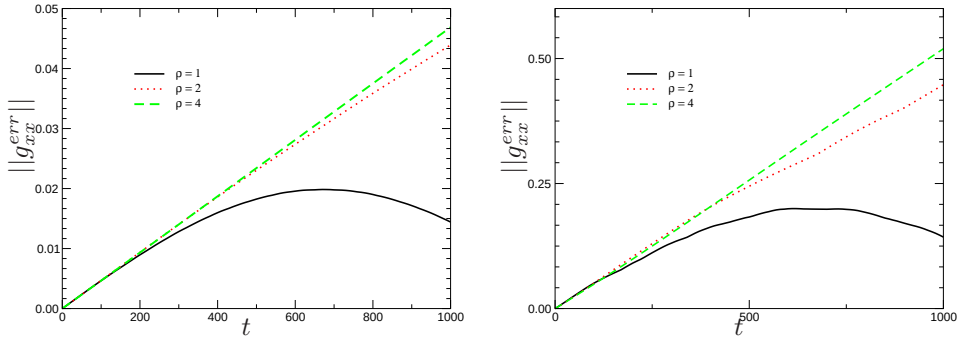

Figure 4. Convergence results for the 1D gauge wave simulation with the Abigel_harm code, for amplitudes of $A = 0.01$ (left) and $A = 0.1$ (right). The graphs show the L_∞ norm of the error in g_{xx}, defined as $g_{xx}^{err} = g_{xx}^{num} - g_{xx}^{ana}$ as a function of time, and rescaled by a factor of $1/\rho^2$. As seen from the graphs, the

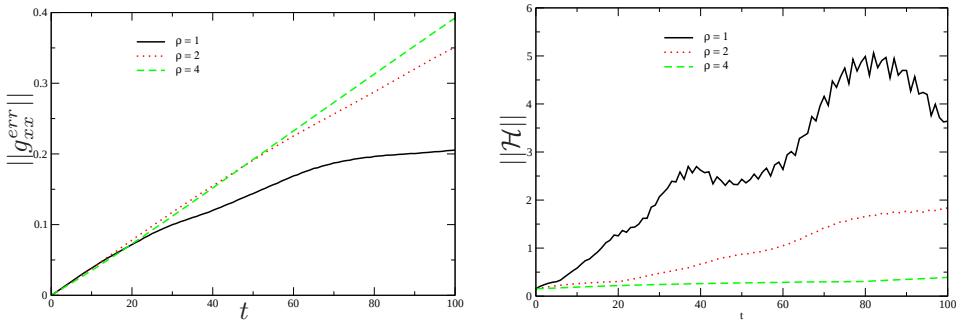

Figure 5. Convergence results for the 2D gauge wave simulation with the Abigel_harm code, for amplitude $A = 0.5$. The left graph shows the L_∞ norm of the error in g_{xx}, rescaled by a factor of $1/\rho^2$, as a function of time; while the right graph shows the same rescaled error norm for the violation of the Hamiltonian constraint $\mathcal{H}$. For the Abigel_harm code, the vanishing of the Hamiltonian constraint is an algebraic identity, making $\mathcal{H}$ of order roundoff. As a result, the constraint violation is super-convergent. The lower amplitude runs revealed no new features.

5.1.3. Results for the KrancNOR System This code picks up a non-constraint violating exponentially growing mode, probably of the form $e^{\lambda t}H$. The error is smooth, with L_2 norm that is 2nd order convergent at early times, but which is super convergent at later times (most likely due to the fact that for the lower gridsizes the error becomes of non-linear amplitude earlier.)

6. Gowdy wave test

The previous three tests involve spacetimes with small curvature. The polarized Gowdy wave test is based upon a strongly curved exact solution. These Gowdy spacetimes describe an expanding vacuum universe containing a plane polarized gravitational wave propagating around a 3-torus T^3 [26]. See [27] for a recent review

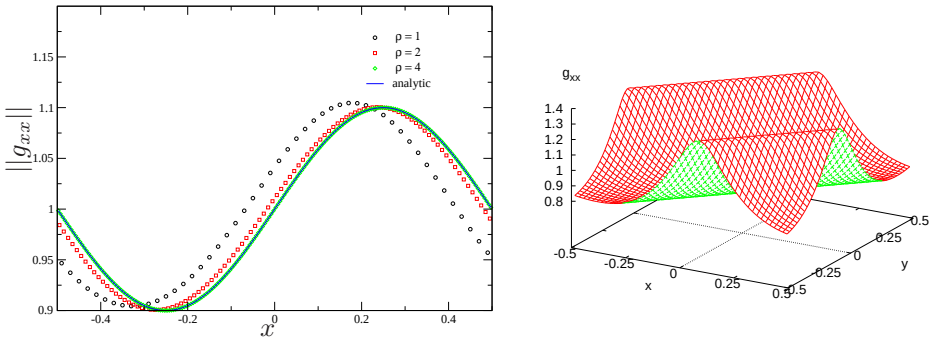

Figure 6. LEFT: Profile of the metric component $g_{xx}(x)$ for the 1D gauge wave with amplitude $A = .1$ at $t = 100$ crossing times, as evolved by the Abigel_harm code. The plot shows, for three different gridsizes, that the phase converges to its analytic value as the grid is refined. RIGHT: Profile of $g_{xx}(x)$ for the 2D gauge wave with amplitude of $A = 0.5$ evolved on the coarsest grid ($\rho = 1$). The (x, y) surface plot shows that $g_{xx}(x)$ is smooth, with no apparent high frequency error modes.

of their properties and studies. The polarized Gowdy metric has the form

$$ds^2 = t^{-1/2}e^{\lambda/2}(-dt^2 + dz^2) + t(e^P dx^2 + e^{-P}dy^2), \tag{21}$$

where $P(t, z)$ and $\lambda(t, z)$ depend periodically on z and satisfy

$$P_{,tt} + t^{-1}\, P_{,t} - P_{,zz} = 0. \tag{22}$$

$$\lambda_{,t} = t\,(P_{,t}^2 + P_{,z}^2) \tag{23}$$

$$\lambda_{,z} = 2\,t\,P_{,z}\,P_{,t}. \tag{24}$$

The shift vanishes, and the lapse is given by

$$\alpha = \sqrt{g_{zz}} = t^{-1/4}e^{\lambda/4}, \tag{25}$$

which satisfies the Bona-Masso-style evolution equation (A.25), or alternatively

$$\partial_t \alpha = -trK\alpha^2 - \alpha/t. \tag{26}$$

The test is based upon the solution [28]

$$P = J_0(2\pi t)\cos(2\pi z), \tag{27}$$

$$\begin{aligned}\lambda \;=\; & -2\pi t J_0(2\pi t)J_1(2\pi t)\cos^2(2\pi z) + 2\pi^2 t^2\left[J_0^2(2\pi t) + J_1^2(2\pi t)\right] \\ & - \tfrac{1}{2}\left\{(2\pi)^2\left[J_0^2(2\pi) + J_1^2(2\pi)\right] - 2\pi J_0(2\pi)J_1(2\pi)\right\},\end{aligned} \tag{28}$$

expressed in terms of the Bessel functions J_n.

The time coordinate t has been chosen such that time increases as the universe expands. Note that the metric has a cosmological type singularity at $t = 0$. However, the test is run in *both* future and past time directions in order to measure performance in both collapsing and expanding situations. The motivation for this is that according to analytical studies [29] and numerical experiments [23], [30] the sign of the extrinsic curvature may have important consequences for triggering or damping constraint violating instabilities.

The qualitative behavior of the solution can be characterized by noting that P slowly decays to zero while λ grows linearly due to the cosmological expansion, and

both P and λ exhibit gravitational wave oscillations. The non-vanishing components of extrinsic curvature,

$$\begin{aligned} K_{xx} &= -\frac{1}{2}t^{1/4}e^{-\lambda/4}e^{P}(1+tP_{,t}), \\ K_{yy} &= -\frac{1}{2}t^{1/4}e^{-\lambda/4}e^{-P}(1-tP_{,t}), \\ K_{zz} &= \frac{1}{4}t^{-1/4}e^{\lambda/4}(t^{-1}-\lambda_{,t}), \end{aligned} \tag{29}$$

do not have a fixed sign but the trace,

$$trK = -\frac{1}{4}t^{1/4}e^{-\lambda/4}(3t^{-1}+\lambda_{,t}), \tag{30}$$

is negative and decays in absolute value consistent with the cosmological expansion

The linear growth of λ leads to exponential growth of g_{zz}. This adds to the difficulty of evolution with a 3D code, as compared with the direct 1D evolution of P used in numerical studies of the approach to the cosmological singularity [31].

The grid is chosen analogous to the 1D wave tests:

- Simulation domain: $z \in [-0.5; +0.5]$, $x = y = 0$
- Grid: $z_n = -0.5 + (n - \frac{1}{2})dz, \quad n = 1 \ldots 50\rho, \quad dz = 1/(50\rho), \quad \rho = (1, 2, 4)$
- Time step: $dt = dz/4 = 0.005/\rho$
- Run time: $t = 1000$, i.e., 1000 crossing times or until code crash.

The (coordinate) velocity of light is constant in the coordinates of (21) so that for a fixed spatial discretization dz the Courant condition is consistent with a fixed timestep dt. This makes the gauge (21) convenient for evolving in the *expanding* direction. For this forward evolution, the initial time is set at $t = 1$ to provide initial data of order unity and the lapse is chosen to correspond to (25). The exponential growth in the metric can trigger an early crash so that code accuracy is tested in a harsh situation. This is illustrated by the various code results shown in Fig. 7.

For runs in the collapsing direction, the approach to the singularity at $t = 0$ is prolonged by evolving with a harmonic time slicing, as previously done by Garfinkle [32]. The harmonic time coordinate τ, given by $F(\tau) := ke^{c\tau} = t$, has lapse

$$\hat{\alpha}(\tau) = ck^{3/4}e^{3c\tau/4+\lambda(F(\tau),z)/4}. \tag{31}$$

The free constants c, k are chosen to start the collapse slowly and to simplify the initial data. We choose the initial time so that $\tau_0 = t_0$ and pick $t_0 \sim 9.8753205829098$, corresponding to the 20th zero of the Bessel function, $J_0(2\pi t_0) = 0$, so that (28) implies $\hat{\alpha}$ is independent of z. This allows us to initialize $\hat{\alpha}_0 = 1$ by setting

$$c \sim 0.0021195119214617, \quad k \sim 9.6707698127638.$$

This places the initial slice far from the cosmological singularity, but not so far that we have to deal with extremely large numbers. The initial values of the metric components are $g_{xx} = g_{yy} = t_0$, $g_{zz} \sim 2.283 \times 10^3$. This challenges a numerical code to accurately track a small effect (the dynamics in g_{xx} and g_{yy}) together with a larger effect (the dynamics in g_{zz}). Typical code results are shown in Fig. 8. Other choices of initial data are of course possible, and certainly worth exploring. The current choice seems to provide a standard testbed capable of good discrimination between different formulations.

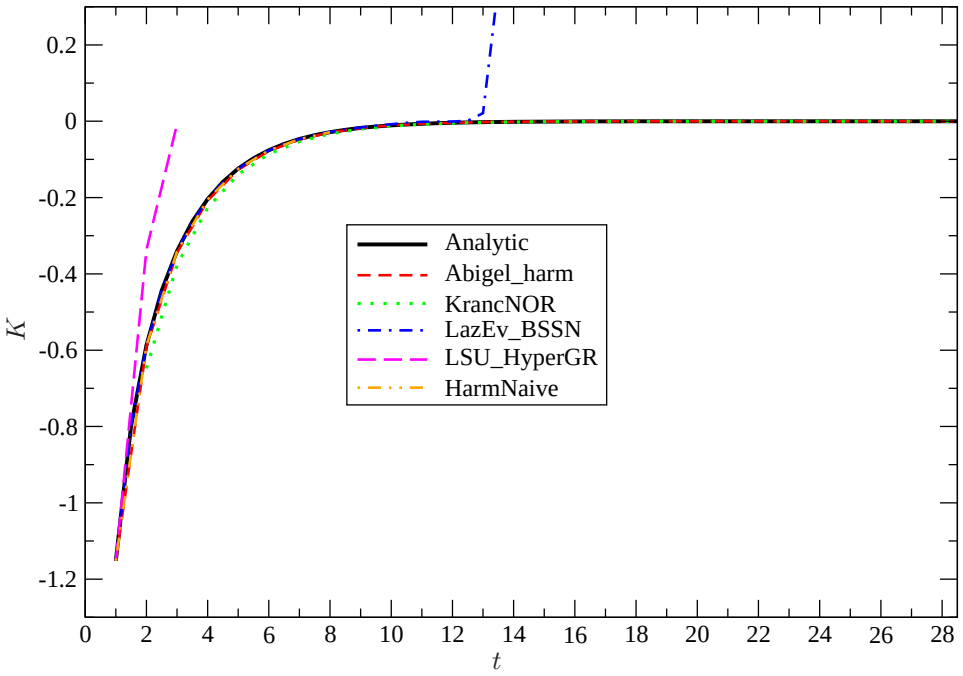

Figure 7. Comparison plots of the trace of the extrinsic curvature K for the polarized Gowdy wave evolved in the expanding direction with the $\rho = 4$ resolution. Analytically K is spatially homogeneous; the plots show its maximum value over the numerical grid.

Both results, for the expanding (Fig. 7) and collapsing (Fig. 8) directions show that the test is able to discriminate between different codes. We observe, as in the gauge wave test, that BSSN-based codes show a less satisfactory performance. Interestingly, the collapsing direction clearly discriminates between different BSSN-based codes.

7. Conclusions

This first round of tests, although modest in scope is a good start at establishing the methods for code verification that have been deemed necessary for any complicated computational discipline, such as numerical relativity, to fulfill its scientific potential. As observed by Post and Votta [33] in their study of the verification and validification of large scale computational projects, "the peer review process in computational science generally doesn't provide as effective a filter as it does for experiment or theory. Many things that a referee cannot detect could be wrong with a computational science paper.... The few existing studies of error levels in scientific computer codes indicate that the defect rate is about seven faults per 1000 lines of Fortran". Their observations are especially pertinent for numerical relativity where validation by agreement with experiment is not available.

Several problems have been encountered in the course of this project. One problem was getting prompt response from a broad set of groups with many other

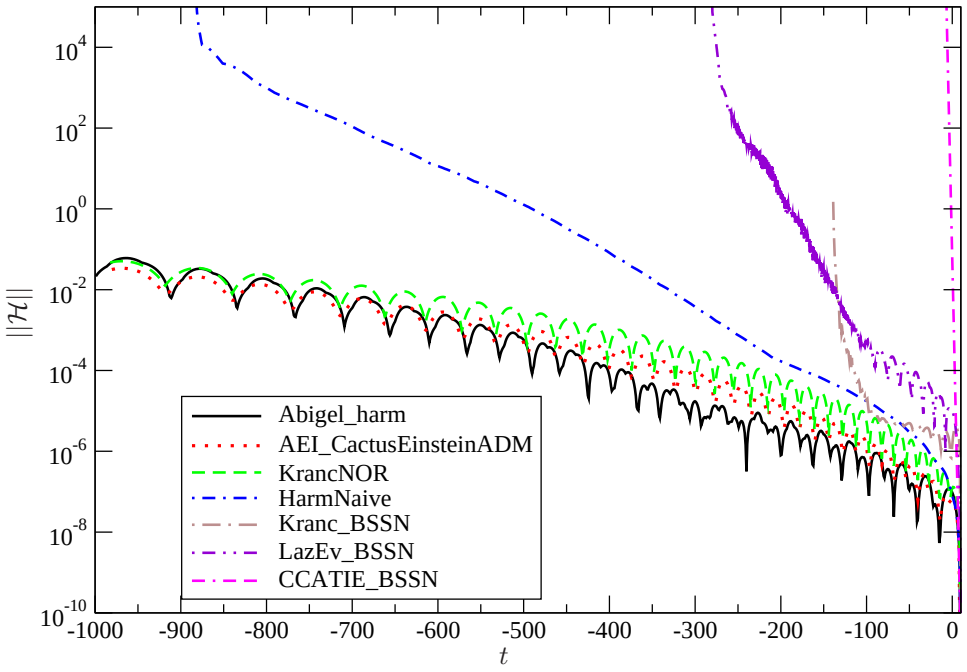

Figure 8. Comparison plot of the L_∞ norm of the Hamiltonian constraint for the polarized Gowdy Wave evolved in the collapsing direction with the $\rho = 4$ resolution.

pressures. The AppleswithApples workshops were very successful in this regard and were absolutely essential in jump-starting and continuing the project. But after the participants dispersed from the workshops, outside pressures led to predictable difficulties. Besides teaching and administrative duties, the overriding scientific pressure in the field has been solving the two black hole problem and supplying waveforms. This raises a complicated juggling of priorities between black hole simulations and code verification. In order for code verification to be attractive, the tests have to be useful and the investment in time has to be minimal. This adds emphasis on the need for tests that are simple to carry out and simple to document the results.

Another level of complication in this project arose from the feedback between test design and the analysis of test output. We have been led in this way to improvements in the tests and to their better understanding. In the robust stability test the correct interpretation of results for weakly hyperbolic algorithms required rethinking the proper choice of norm and refinement procedure for judging stability. In the gauge wave tests, the desire for computational efficiency in detecting nonlinear problems at an early time has led us to the recommendation of a higher amplitude $A = .5$ for the test, as opposed to the original specifications $A = .01$ and $A = .1$.

The robust stability test is presented as a pass/fail test. For the linear wave and gauge wave tests the amplitude and phase errors in the output data for the wave profile provide a good comparison of code performance. For the Gowdy test, there were unanticipated shortcomings in the output content that should lend valuable experience

in the design of future black holes tests. Useful benchmarks have been established for the linear wave, gauge wave, and Gowdy wave tests, which have revealed clear deficiencies in various codes. Such deficiencies raise a clear alert that it is necessary to apply or recheck other verification techniques, such as convergence tests.

These first round results provide a good basis for proposing new tests. In another project utilizing the gauge wave test, a shifted version of the test has also been formulated and studied [24, 34]. This new test involving a shift vector fills a gap in the four original tests for periodic boundary conditions. A second round of boundary tests based upon the periodic tests have been proposed. The specifications are given on the Alliance website [5]. Results of some of these boundary tests have been reported elsewhere [25, 35]. The next stage is to formulate tests involving black holes.

The code comparisons have proved useful for designing code improvements and for stimulating other new developments. During the course of this work, results of the shifted gauge wave test were key to recognizing the importance of discrete energy and flux conservation for harmonic code performance [24]. The need to carry out the tests with a wide range of formulations has led to the development of symbolic code generation [36]. Although the tests were designed for finite difference codes, they have been adapted and applied to pseudo-spectral codes [34]. Further independent studies based upon the tests have played a major part in thesis research [37, 38].

Establishment of the CVS data repository has been an important step in the documentation of test results. Instructions for accessing the data are given at [5]. The CVS directory structure has been significantly streamlined and documented since the beginning of the project. However, the difficulties in completing this analysis of the first round of tests has emphasized the need of a uniform standard for data structures and output. Rather than trying to anticipate a complete list of useful output quantities, it seems more desirable to output the 3-metric and extrinsic curvature at specified times. Then other output quantities can be constructed in post processing. Ideally, this should be done in some standardized way using automated routines and graphical interfaces. All of this would require considerable infrastructure to provide hardware for data storage and software for processing. This is one of the important matters that will be presented for discussion at future Alliance meetings.

Acknowledgments

We are grateful to UNAM in Mexico City, to the University of Cordoba, and to the Center for Computation & Technology at Louisiana State University for their hospitality in conducting AwA workshops. M.C.B, S.H., C.L., E.S., and J.W. gratefully acknowledge hospitality of the Albert Einstein Institute, and S.H. of the University of the Balearic Islands. We benefited from discussions with Daniela Alic, Miguel Alcubierre, Adel Benlagra, Carles Bona, Helmut Friedrich, Ian Hawke, Frank Herrmann, Carlos Palenzuela, Oscar Reula, Krzysztof Roszkowski, Marcelo Salgado, Hisa-aki Shinkai, Manuel Tiglio, and Tilman Vogel. The work of M.C.B and J.W. was supported by NSF grant PH-0553597 to the University of Pittsburgh. Y.Z. was supported by NFS grants PHY-0722315, PHY-0722703, PHY-0714388, and PHY-653303, and by the NASA Center for Gravitational Wave Astronomy at the University of Texas at Brownsville (NAG5-13396).

Appendix A. Code descriptions

Appendix A.1. Standard ADM: Kranc_FreeADM, and AEI_CactusEinsteinADM codes

The formulation of the Einstein equation by Arnowitt, Deser and Misner (ADM) [39] provides a standard notion for "evolving" space-time as an initial value problem in general relativity, which was initially presented in a Hamiltonian context. What is referred to as a "standard ADM" system in the numerical relativity community is a reformulation due to York [40], which one obtains by 3+1–decomposition of the Einstein tensor (as opposed to 3+1–decomposition of the Ricci tensor in the original ADM version), or equivalently by adding appropriate constraint terms to the evolution equations. As pointed out by Frittelli [41], York's "standard ADM" system does in particular have nicer properties regarding the constraint propagation system. This system is particularly simple, has a long history in numerical relativity and exhibits some typical problems. We therefore use it as the starting point for our numerical comparisons. The evolution equations are

$$\partial_t \gamma_{ij} = -2\alpha K_{ij} + \nabla_i \beta_j + \nabla_j \beta_i \tag{A.1}$$

$$\partial_t K_{ij} = \alpha R^{(3)}_{ij} + \alpha K K_{ij} - 2\alpha K_{ik} K^k{}_j - \nabla_i \nabla_j \alpha + (\nabla_i \beta^k) K_{kj} + (\nabla_j \beta^k) K_{ki} + \beta^k \nabla_k K_{ij}, \tag{A.2}$$

and the constraint equations are

$$\mathcal{H} = \mathcal{H}^{ADM} := R^{(3)} + K^2 - K_{ij} K^{ij}, \tag{A.3}$$

$$\mathcal{M}_i = \mathcal{M}^{ADM}_i := \nabla_j K^j{}_i - \nabla_i K, \tag{A.4}$$

where (γ_{ij}, K_{ij}) are the induced three-metric and the extrinsic curvature, (α, β_i) are the lapse function and the shift covector, ∇_i is the 3-dimensional covariant derivative and $R^{(3)}_{ij}$ is the 3-dimensional Ricci tensor associated with γ_{ij}.

We have tested two implementations of the standard ADM system, the code AEI_CactusEinsteinADM, which is freely available via the website [42], and Kranc_FreeADM which is based on the Cactus Toolkit [42] and Kranc software [36]. AEI_CactusEinsteinADM uses a hardcoded ICN time update scheme (see e.g. [11]), whereas Kranc_FreeADM uses a method of lines (MoL) approach based on the CactusMoL thorn (in practice, RK3, RK4 and ICN (see e.g. [11]) have also been used, as indicated). In all of these codes, spatial partial derivatives are reduced to partial derivatives of the 3-metric, i.e., all expressions such as Christoffel symbols are expanded out. Due to the absence of first-order variables, no further ambiguities arise. Centered second and fourth order discretization is used (see Appendix B.1), and third order Kreiss-Oliger dissipation is optionally applied to all variables (see Appendix B.2).

The hyperbolicity of the ADM free evolution scheme has been analyzed and found to be weakly hyperbolic with the type of gauge conditions that we use [11]. Since many of our tests are essentially 1D tests, where ADM yields good results, we have also analyzed the hyperbolicity of ADM in 1D. For simplicity of presentation we restrict ourselves to the linearized case. Assuming propagation in the x–direction we obtain the following evolution equations. For the off-diagonal components we get

$$\partial_t \gamma_{yz} = 2K_{yz}, \quad \partial_t K_{yz} = \partial_{xx} \gamma_{yz}/2, \quad \partial_t K_{xy} = 0, \quad \partial_t K_{xz} = 0.$$

The evolution equations for γ_{xy} and γ_{xz} are analogous to the evolution equation for γ_{yz}. The fact that the evolution equations for K_{xy} and K_{xz} are trivial renders the evolution system for the off-diagonal components weakly hyperbolic, see e.g. [11]. For the diagonal components we get

$$\partial_t \gamma_{ii} = 2K_{ii} \qquad (i = x, y, z), \tag{A.5}$$

$$\partial_t K_{xx} = \partial_{xx}\alpha + \frac{1}{2}\partial_{xx}(\gamma_{yy} + \gamma_{zz}), \tag{A.6}$$

$$\partial_t K_{jj} = \frac{1}{2}\partial_{xx}\gamma_{jj} \qquad (j = y, z). \tag{A.7}$$

Considering for simplicity the densitized lapse case, $\alpha = \sqrt{\gamma}$, the evolution equation for K_{xx} becomes

$$\partial_t K_{xx} = \frac{1}{2}\partial_{xx}\gamma_{xx} + \partial_{xx}(\gamma_{yy} + \gamma_{zz})$$

and one finds that the diagonal subsystem is only weakly hyperbolic. However, within the subclasses of gauge wave ($\gamma_{yy} = \gamma_{zz} = 0$) or linear wave ($\gamma_{xx} = 0$) data, the 1D ADM system corresponds to copies of the 1D wave equation and is therefore well-posed. The case for the Bona-Masso lapse condition is analogous.

Appendix A.2. Abigel_harm

The Abigel code developed in Pittsburgh is based upon a symmetric hyperbolic formulation of the Einstein equations using generalized harmonic coordinates satisfying the curved space wave equation

$$\Box x^\alpha = \frac{1}{\sqrt{-g}}\partial_\mu(\sqrt{-g}g^{\mu\nu}\partial_\nu x^\alpha) = \frac{1}{\sqrt{-g}}\tilde{H}^\alpha(x^\beta, g_{\rho\sigma}), \tag{A.8}$$

where $\tilde{H}^\alpha$ are harmonic source terms. The original version of the evolution equations was [43]

$$\bar{g}^{\alpha\beta}\partial_\alpha\partial_\beta\bar{g}^{\nu\mu} = S^{\mu\nu} \tag{A.9}$$

where the left hand side is the principle part and the right hand side contains nonlinear first-derivative terms. Here $\bar{g}^{\mu\nu} = \sqrt{-g}g^{\mu\nu}$, with $g = \det(g_{\mu\nu}) = \det(\bar{g}^{\mu\nu})$. and the harmonic constraints $\partial_\nu\bar{g}^{\mu\nu} = \tilde{H}^\mu$ are used in the Einstein equations to eliminate second derivatives in the source terms $S^{\mu\nu}$. For further details concerning the formulation and its implementation see [43].

The code with which the four tests were performed was constructed by rewriting (A.9) in the flux conservative form

$$\partial_\alpha\left(g^{\alpha\beta}\partial_\beta\bar{g}^{\mu\nu}\right) = \tilde{S}^{\mu\nu}. \tag{A.10}$$

and reducing it to the first order in time form

$$\partial_t\bar{g}^{\mu\nu} = -\frac{\bar{g}^{ti}}{\bar{g}^{tt}}\partial_i\bar{g}^{\mu\nu} + \frac{\sqrt{-g}}{\bar{g}^{tt}}Q^{\mu\nu} \tag{A.11}$$

$$\partial_t Q^{\mu\nu} = -\partial_i\left(g^{ij}\partial_j\bar{g}^{\mu\nu} + g^{it}\partial_t\bar{g}^{\mu\nu}\right) + \tilde{S}^{\mu\nu} \tag{A.12}$$

$$= -\partial_i\left[\left(g^{ij} - \frac{g^{ti}g^{tj}}{g^{tt}}\right)\partial_j\bar{g}^{\mu\nu}\right] - \partial_i\left(\frac{g^{it}}{g^{tt}}Q^{\mu\nu}\right) + \tilde{S}^{\mu\nu} \tag{A.13}$$

$$= -\partial_i\left(h^{ij}\partial_j\bar{g}^{\mu\nu}\right) - \partial_i\left(\frac{g^{it}}{g^{tt}}Q^{\mu\nu}\right) + \tilde{S}^{\mu\nu} \tag{A.14}$$

in terms of the evolution variables $(\bar{g}^{\mu\nu}, Q^{\mu\nu})$, where

$$Q^{\mu\nu} = g^{t\alpha}\partial_\alpha \bar{g}^{\mu\nu} \tag{A.15}$$

and $h^{ij} = g^{ij} - g^{it}g^{jt}/g^{tt}$ is the spatial 3-metric. Centered derivatives are used to finite difference (A.11) and the source terms $\tilde{S}^{\mu\nu}$ in (A.14). The remaining part of Eq. (A.14) is finite-differenced as follows:

$$g^{\alpha\beta}_{[I+1/2,J,K]} = \frac{A_{+x}\bar{g}^{\alpha\beta}_{[I,J,K]}}{\sqrt{-A_{+x}g_{[I,J,K]}}} + \mathcal{O}(\Delta^2) \tag{A.16}$$

$$h^{ij}_{[I+1/2,J,K]} = g^{ij}_{[I+1/2,J,K]} - \frac{g^{ti}_{[I+1/2,J,K]}\, g^{tj}_{[I+1/2,J,K]}}{g^{tt}_{[I+1/2,J,K]}} \tag{A.17}$$

$$\partial_x\left(h^{xx}\partial_x\bar{g}^{\mu\nu}\right)_{[I,J,K]} = D_{-x}\left(h^{xx}_{[I+1/2,J,K]}\; D_{+x}\bar{g}^{\mu\nu}_{[I,J,K]}\right) + \mathcal{O}(\Delta^2) \tag{A.18}$$

$$\partial_x\left(h^{xy}\partial_y\bar{g}^{\mu\nu}\right)_{[I,J,K]} = D_{-x}\left(h^{xx}_{[I+1/2,J,K]}\; A_{+x}D_{0y}\bar{g}^{\mu\nu}_{[I,J,K]}\right) + \mathcal{O}(\Delta^2) \tag{A.19}$$

$$\partial_x\left(\frac{g^{xt}}{g^{tt}}Q^{\mu\nu}\right)_{[I,J,K]} = D_{-x}\left(\frac{g^{xt}_{[I+1/2,J,K]}}{g^{tt}_{[I+1/2,J,K]}}\; A_{+x}Q^{\mu\nu}_{[I,J,K]}\right) + \mathcal{O}(\Delta^2) \tag{A.20}$$

where the averaging operator A_{+x} is defined in Appendix B.1. The code is evolved as a first differential order in time and second order in space system with a 2-step iterated Crank-Nicholson algorithm.

Appendix A.3. HarmNaive

The HarmNaive code is based upon harmonic coordinates but differs from the Abigel_harm code because the evolution system consists of only the 6 wave equations (A.10) for the spatial components $\bar{g}^{ij}$. The time components are propagated by the harmonic conditions (A.8), i.e.

$$\partial_t\bar{g}^{\alpha t} + \partial_i\bar{g}^{\alpha i} = \hat{H}^\alpha. \tag{A.21}$$

The coupling between $\bar{g}^{ij}$ and $\bar{g}^{\alpha t}$ makes the system only weakly hyperbolic.

The evolution equations for $\bar{g}^{ij}$ and Q^{ij} are finite differenced as in the Abigel_harm code. The evolution equation (A.21) for $\bar{g}^{\alpha t}$ is approximated by central differences. The update scheme is a 2-step iterative Crank-Nicholson algorithm.

Appendix A.4. KrancNOR code

Appendix A.4.1. Continuum formulation Nagy, Ortiz and Reula suggested [17] modifications to the ADM system such that it can be made strongly hyperbolic whilst remaining in second order form. The system we use includes the slight adjustments of [9]. Additionally, we use an evolved lapse. The variable f_i is defined as

$$f_i = \gamma^{kl}(\gamma_{ik,l} - \frac{1}{2}\rho\gamma_{kl,i}) \tag{A.22}$$

with parameter ρ. This introduces the new constraint G_i where

$$G_i := f_i - \gamma^{kl}(\gamma_{ik,l} - \frac{1}{2}\rho\gamma_{kl,i}). \tag{A.23}$$

Starting from the ADM evolution equations, an evolution equation for f_i is obtained by differentiating (A.22) and commuting space and time derivatives. The

Hamiltonian and momentum constraints are added with parameters c and b, and derivatives of the G_i are added with parameters a and a':

$$\begin{aligned}
\partial_t \gamma_{ij} &= -2\alpha K_{ij} \\
\partial_t K_{ij} &= -D_i D_j \alpha + \alpha(R^{(3)}_{ij} - 2K_{ik}K^k{}_j + K_{ij}K) + \frac{a}{2}G_{(i,j)} + (c\mathcal{H} + a' G_{k,l}\gamma^{kl})\gamma_{ij} \\
\partial_t f_i &= \alpha K^{kl}(2\gamma_{ik,l} - \rho\gamma_{kl,i}) - \gamma^{kl}\left[2(\alpha K_{ik})_{,l} - \rho(\alpha K_{kl})_{,i}\right] + 2b\mathcal{M}_i \\
\partial_t \alpha &= -\alpha F(\alpha, K, x^i).
\end{aligned}$$

The variables γ_{ij}, K_{ij}, f_i and α are evolved. Due to the symmetries of γ_{ij} and K_{ij}, this leads to 16 evolved variables. We write the Ricci tensor entirely in terms of γ_{ij}; f_i is only used where it appears as part of G_i.

For those tests requiring harmonic slicing, the lapse source function is

$$F(\alpha, K, x^i) = \alpha K \tag{A.24}$$

and for the expanding Gowdy test,

$$F(\alpha, K, x^i) = K_{33}/\alpha \tag{A.25}$$

which is compatible with the exact lapse in this case. We make the following choice of parameters:

$$a = 1, \quad b = 1, \quad a' = 0, \quad \rho = 2/3, \quad c = 0. \tag{A.26}$$

Note that choosing parameters

$$a = 0, \quad b = 0, \quad a' = 0, \quad \rho = 0, \quad c = 0 \tag{A.27}$$

leads to a standard ADM system. This is useful for testing the code.

Appendix A.4.2. Semi-discrete scheme To form the semi-discrete approximation, discretization in space is performed according to the standard second order accurate discretization B.1. Finite differences are taken only of the evolved variables γ_{ij}, K_{ij}, f_i and α. This means that where derivatives of other quantities appear, they are explicitly written in terms of derivatives of the evolved variables (e.g. by using the Leibniz rule). We do not add Kreiss-Oliger type artificial dissipation, as it was not necessary for stability.

Appendix A.4.3. Time integration Time integration is performed using the method of lines with the iterative Crank-Nicholson (ICN) method.

Appendix A.4.4. Output For our state vector $v = (\gamma_{ij}, K_{ij}, f_i)^T$ we define the L_2 and D_+ norms:

$$\|v\|^2_{L_2} \equiv \sum_{\text{grid}} (\eta^{ik}\eta^{jl}\gamma_{ij}\gamma_{kl} + \eta^{ik}\eta^{jl}K_{ij}K_{kl} + \eta^{ij}f_i f_j)h^3 \tag{A.28}$$

$$\|v\|^2_{D_+} \equiv \|v\|^2_{L_2} + \sum_{\text{grid}} (\eta^{ik}\eta^{jl}\eta^{mn}D_{+m}\gamma_{ij}D_{+n}\gamma_{kl})h^3 \tag{A.29}$$

where $\eta \equiv \text{diag}(1,1,1)$. This is the norm obtained from a reduction to first order [11] of the semi-discrete equations. The exact solution is denoted $u^n_j \equiv u(t^n, x_j)$ and the error is defined as

$$E \equiv v - u. \tag{A.30}$$

For the stability test, the exact solution is taken to be Minkowski in Cartesian coordinates. For those tests which are perturbations of this solution, we analyze relative error with respect to this background. We denote the background solution as u_B. Hence the relative error about this background is

$$r \equiv \frac{\|E\|_{L_2}}{\|u - u_B\|_{L_2}}. \tag{A.31}$$

In general, we run until this quantity exceeds 0.2 (a relative error of 20%).

Appendix A.5. Family of BSSN (Shibata-Nakamura and Baumgarte-Shapiro) formulations

The family of BSSN systems is constituted by variations of an evolution system that had originally been proposed by Nakamura in the late 80s, and has been subsequently modified by Nakamura-Oohara and Shibata-Nakamura [44, 45, 46], and later by various other authors. The formulation is characterized by introducing a contracted connection term as a new variable, a conformal decomposition of the metric and extrinsic curvature variables, and adding constraints to the evolution equations. In particular, the system can be viewed as the NOR-system plus a conformal decomposition which leads to the evolution of a unimodular metric. The advantage of this formulation was re-announced by Baumgarte and Shapiro [47]. Modifications of the system have been obtained by variations in how derivatives of the new variables are written, how the gauge is specified, how algebraic constraints are treated, and the way (differential or algebraic) constraints are added to the evolution equations. A detailed discussion of well-posedness for the BSSN family has been given by Gundlach and Martin-Garcia [8, 9, 10], to which we refer for details about the BSSN family. The set of evolved variables are the logarithm of the conformal factor φ, the conformally rescaled three-metric $\tilde{\gamma}_{ij}$, the trace of the extrinsic curvature K, the conformally rescaled traceless extrinsic curvature $\tilde{A}_{ij}$, and the contracted Christoffel symbols $\tilde{\Gamma}^i$:

$$\varphi = (1/12)\log(\det\gamma_{ij}), \tag{A.32}$$

$$\tilde{\gamma}_{ij} = e^{-4\varphi}\gamma_{ij}, \tag{A.33}$$

$$K = \gamma^{ij}K_{ij}, \tag{A.34}$$

$$\tilde{A}_{ij} = e^{-4\varphi}(K_{ij} - (1/3)\gamma_{ij}K), \tag{A.35}$$

$$\tilde{\Gamma}^i = \tilde{\Gamma}^i_{jk}\tilde{\gamma}^{jk}. \tag{A.36}$$

This immediately leads to the two algebraic constraints

$$\det\gamma_{ij} = 1, \qquad \tilde{A}^i_i = 0 \tag{A.37}$$

and the differential constraint

$$\tilde{\Gamma}^i - \tilde{\gamma}^{jk}\tilde{\Gamma}^i_{jk} = 0, \tag{A.38}$$

which are again propagated by the evolution equations. Note that densitized quantities (those with a tilde) have their indices raised and lowered with the conformally rescaled three-metric $\tilde{\gamma}_{ij}$.

The standard Hamiltonian and momentum constraints (A.3,A.4) and (A.4) can be expressed in the BSSN variables as

$$\mathcal{H} = e^{-4\varphi}\tilde{R} - 8e^{-4\varphi}\tilde{D}^j\tilde{D}_j\varphi - 8e^{-4\varphi}(\tilde{D}^j\varphi)(\tilde{D}_j\varphi) + (2/3)K^2 - \tilde{A}_{ij}\tilde{A}^{ij} - (2/3)\mathcal{A}K, \tag{A.39}$$

$$\mathcal{M}_i = 6\tilde{A}^j{}_i(\tilde{D}_j\varphi) - 2\mathcal{A}(\tilde{D}_i\varphi) - (2/3)(\tilde{D}_iK) + \tilde{\gamma}^{kj}(\tilde{D}_j\tilde{A}_{ki}). \tag{A.40}$$

The BSSN evolution equations, which are obtained from the ADM equations (A.1 - A.4) by using the definitions (A.32 - A.36) and making a standard choice for adding constraints, are

$$\begin{aligned}
\mathcal{L}_n\varphi &= -(1/6)\alpha K, && \text{(A.41)}\\
\mathcal{L}_n\tilde{\gamma}_{ij} &= -2\alpha\tilde{A}_{ij}, && \text{(A.42)}\\
\mathcal{L}_n K &= -D^i D_i\alpha + \alpha\tilde{A}_{ij}\tilde{A}^{ij} + (1/3)\alpha K^2, && \text{(A.43)}\\
\mathcal{L}_n\tilde{A}_{ij} &= -e^{-4\varphi}(D_iD_j\alpha)^{TF} + e^{-4\varphi}\alpha(R^{BSSN}_{ij})^{TF} + \alpha K\tilde{A}_{ij} - 2\alpha\tilde{A}_{ik}\tilde{A}^k{}_j, && \text{(A.44)}\\
\mathcal{L}_n\tilde{\Gamma}^i &= -2(\partial_j\alpha)\tilde{A}^{ij} + 2\alpha\big(\tilde{\Gamma}^i_{jk}\tilde{A}^{kj} - (2/3)\tilde{\gamma}^{ij}(\partial_j K) + 6\tilde{A}^{ij}(\partial_j\varphi)\big), && \text{(A.45)}
\end{aligned}$$

where $\tilde{D}_i$ is the covariant derivative associated with $\tilde{\gamma}_{ij}$, and $\mathcal{L}_n = \partial_t - \mathcal{L}_\beta$ is the Lie derivative along the unit normal. Note that $\int \mathcal{L}_n K d^3x$ is positive definite apart from boundary terms involving the lapse (which vanish for periodic boundary conditions). The Ricci curvature R^{BSSN}_{ij} in terms of the BSSN variables becomes

$$\begin{aligned}
R^{BSSN}_{ij} &= \tilde{R}_{ij} + R^{\varphi}_{ij},\\
R^{\varphi}_{ij} &= -2\tilde{D}_i\tilde{D}_j\varphi - 2\tilde{\gamma}_{ij}\tilde{D}^k\tilde{D}_k\varphi + 4(\tilde{D}_i\varphi)(\tilde{D}_j\varphi) - 4\tilde{\gamma}_{ij}(\tilde{D}^k\varphi)(\tilde{D}_k\varphi),\\
\tilde{R}_{ij} &= -(1/2)\tilde{\gamma}^{lk}\partial_l\partial_k\tilde{\gamma}_{ij} + \tilde{\gamma}_{k(i}\partial_{j)}\tilde{\Gamma}^k + \tilde{\Gamma}^k\tilde{\Gamma}_{(ij)k} + 2\tilde{\gamma}^{lm}\tilde{\Gamma}^k_{l(i}\tilde{\Gamma}_{j)km} + \tilde{\gamma}^{lm}\tilde{\Gamma}^k_{im}\tilde{\Gamma}_{klj}.
\end{aligned}$$

Note that there are different ways to numerically compute the trace free part of the Ricci tensor, e.g. one can project out the trace of the Ricci tensor according to

$$R^{TF}_{ij} = R_{ij} - \frac{1}{3}R\gamma_{ij}, \tag{A.46}$$

compute the Ricci Scalar from the Hamiltonian constraint (A.39), or compute the trace free part explicitly by assuming the algebraic constraints hold. We refer to the code descriptions below for details concerning the individual codes. In summary, the fundamental dynamical variables in BSSN are ($\varphi, \tilde{\gamma}_{ij}$, K,$\tilde{A}_{ij}$,$\tilde{\Gamma}^i$), which total 17. The 4 gauge quantities are (α, β^i), and the 9 constraint components are ($\mathcal{H}, \mathcal{M}_i, \mathcal{G}^i, \mathcal{A}, \mathcal{S}$), i.e., 9 components.

Appendix A.5.1. Concrete implementations We have compared a number of codes based on variants of the BSSN system. Several of these are based on the Cactus computational toolkit [42]: the CCATIE_BSSN [48, 49] and Kranc_BSSN [50] codes, and the LazEv_BSSN [51] code. Of these, CCATIE_BSSN and Kranc_BSSN use the CactusMoL time integrator, which provides the RK3, RK4 and ICN methods, among others (see e.g. [11]). Kranc_BSSN is based on the Kranc code generation software package [36]. All codes use straightforward replacement of partial derivatives by standard second order centered finite differences with a three point stencil (most codes are also able to use standard centered fourth order finite differencing).

Most of the BSSN codes have a long history of use in production environments and have a large number of parameters that allow them great flexibility, e.g. regarding details of the numerical methods, gauge conditions, or the way the algebraic constraints are treated. Typical options to solve the algebraic constraints at every intermediate timestep use the following replacements:

- Ensure that $\tilde{\gamma}_{ij}$ has unit determinant by setting

$$\tilde{\gamma}_{ij} \to \frac{\tilde{\gamma}_{ij}}{\det\tilde{\gamma}^{1/3}}. \tag{A.47}$$

- Ensure that $\tilde{A}_{ij}$ remains trace-free by setting

$$\tilde{A}_{ij} \to \tilde{A}_{ij} - \frac{1}{3}\tilde{A}_{lm}\tilde{\gamma}^{il}\tilde{\gamma}^{jm}. \tag{A.48}$$

- Divide $\tilde{A}_{ij}$ by the same factor that is used to remove the determinant of $\tilde{\gamma}_{ij}$:

$$\tilde{A}_{ij} \to \frac{\tilde{A}_{ij}}{\det \tilde{\gamma}^{1/3}}. \tag{A.49}$$

Note that an ambiguity arises whenever a Γ^i or a $\tilde{\gamma}^{kj}\gamma_{ij,k}$ occurs, as they are related analytically by the equation $\Gamma^i = -\gamma^{ij}{}_{,j} - \frac{1}{2}\gamma^{il}(\ln\gamma)_{,l}$. If the constraint $\gamma = 1$ holds, e.g. if it is enforced at each timestep, this is equivalent numerically (up to round-off error) to $\Gamma^i = -\gamma^{ij}{}_{,j}$. Some authors replace $\gamma^{ij}{}_{,j}$ using $-\Gamma^i$ only when the expression appears under a derivative, but more complicated rules have also been applied.

Appendix A.6. KrancFN

Appendix A.6.1. Continuum formulation The Friedrich-Nagy system [52] is a frame-based first order formulation that has been shown to yield a well-posed initial boundary value problem. The formulation starts from the four dimensional vacuum equations

$$T_{IJ}{}^{\mu} := [e_I, e_J]^{\mu} - (\Gamma_I{}^K{}_J - \Gamma_J{}^K{}_I)e_K{}^{\mu} = 0, \quad \mu = 0,1,2,3 \tag{A.50}$$

$$\Delta_{IJKL} := R_{IJKL}(\Gamma) - C_{IJKL} = 0 \tag{A.51}$$

$$H_{JKL} := \nabla_I C_{JKL}{}^I = 0, \qquad I = 0,1,2,3 \tag{A.52}$$

where e_I denote the tetrad vectors with coordinate components $e_I{}^{\mu}$, $\Gamma_I{}^K{}_J$ are the connection coefficients defined by $\nabla_{e_I} e_K = \Gamma_I{}^J{}_K e_J$ and satisfying $\eta_{JM}\Gamma_I{}^J{}_K + \eta_{KJ}\Gamma_I{}^J{}_M = 0$. R_{IJKL} and C_{IJKL} denote the components of the Riemann and Weyl tensor with respect to the tetrad. The Riemann tensor is given in terms of the connection coefficients by

$$\begin{aligned} R_{IJ}{}^L{}_K(\Gamma) = {} & e_I(\Gamma_J{}^L{}_K) - e_J(\Gamma_I{}^L{}_K) \\ & -\Gamma_M{}^L{}_K\Gamma_I{}^M{}_J - \Gamma_I{}^M{}_K\Gamma_J{}^L{}_M + \Gamma_M{}^L{}_K\Gamma_J{}^M{}_I + \Gamma_I{}^L{}_M\Gamma_J{}^M{}_K. \end{aligned} \tag{A.53}$$

Eq. (A.50) states that the connection is torsion free, Eq. (A.51) are the vacuum Einstein equations and Eq. (A.52) is the Bianchi identity for a vacuum spacetime. From Eqs. (A.50) – (A.52), a symmetric hyperbolic evolution system is obtained by choosing certain combinations of components of the above equations as well as a gauge that is adapted to the boundary.

Assuming a boundary at $z = const$, we foliate the interior domain by time-like hypersurfaces T_c given by $z = c = const$. The frame is adapted to this foliation and boundary such that the frame vector e_3 is orthogonal to T_c, which implies for the coordinate components

$$e_a{}^3 = 0, \quad a = 0,1,2, \quad e_3{}^3 > 0. \tag{A.54}$$

e_3 being the unit normal to T_c implies $\Gamma_a{}^3{}_b = \Gamma_{(a}{}^3{}_{b)}$.

The mean extrinsic curvature of T_c is prescribed as a function of the coordinates $f(x^{\mu})$ and used to eliminate the connection coefficient $\Gamma_0{}^3{}_0$ from the equations,

$$\Gamma_0{}^3{}_0 = f + \Gamma_1{}^3{}_1 + \Gamma_2{}^3{}_2. \tag{A.55}$$

The variation of e_0 within T_c is prescribed by functions $F^A(x^\mu)$, $A = 1, 2$ according to $D_{e_0} e_0 = F^A e_A$, where D denotes the induced connection on T_c. This eliminates the connection coefficients

$$\Gamma_0{}^A{}_0 = F^A, \quad A = 1, 2. \tag{A.56}$$

The tetrad vectors e_A are Fermi-transported along e_0 with respect to D and therefore

$$\Gamma_0{}^A{}_B = 0, \quad A, B = 1, 2. \tag{A.57}$$

The coordinates $\{x^\mu\}$ are chosen such that the tetrad vector e_0 represents the time flow ∂_t, i.e.,

$$e_0{}^\mu = \delta_0{}^\mu. \tag{A.58}$$

The ten independent components of the Weyl tensor are encoded in the symmetric and tracefree tensor fields

$$E_{ij} := C_{i0j0}, \qquad B_{ij} := \frac{1}{2} C_{0ikl}\,{}^{(3)}\epsilon^{kl}{}_j$$

corresponding to the electric and magnetic parts with respect to e_0. The conditions $\delta^{ij} E_{ij} = \delta^{ij} B_{ij} = 0$ are incorporated explicitly by eliminating

$$E_{33} = -(E_{11} + E_{22}), \quad B_{33} = -(B_{11} + B_{22}) \tag{A.59}$$

from the equations. In total the Friedrich-Nagy system has 37 variables, namely

$$\mathbf{u} = (e_A{}^p, e_3{}^\mu, \Gamma_i{}^0{}_j, \Gamma_3{}^i{}_j, \Gamma_{(A}{}^3{}_{B)}, \Gamma_A{}^B{}_C, E_{iA}, B_{iA})^T, \tag{A.60}$$

where

$$A, B, C = 1, 2, \quad i, j = 1, 2, 3, \quad p = 0, 1, 2, \quad \mu = 0, 1, 2, 3.$$

A symmetric hyperbolic evolution system for the variables (A.60) is obtained by taking the following combinations of Eqs. (A.50) – (A.52):

$$T_{0A}{}^p = 0, \quad T_{03}{}^\mu = 0, \quad \Delta_{0Bab} = 0, \quad \Delta_{0131} = 0, \quad \Delta_{0232} = 0,$$
$$\Delta_{0132} + \Delta_{0231} = 0, \quad \Delta_{0130} + \Delta_{1232} = 0, \quad \Delta_{0230} + \Delta_{2131} = 0,$$
$$\Delta_{AB03} = 0, \quad \Delta_{A003} = 0, \quad \Delta_{3A03} + \Delta_{303A} = 0, \quad \eta^{ab}\Delta_{3ab3} = 0,$$
$$H_{0ij} - \frac{1}{2}\delta^3{}_{(i}\epsilon_{j)}{}^{3l} H_{mn0}\,\epsilon^{mn}{}_l = 0, \quad \frac{1}{2} H_{mki}\,\epsilon^{mk}{}_j + \delta^3{}_{(i}\epsilon_{j)}{}^{3m}\, H_{0m0} = 0$$

where the convention for the indices is the same as in Eq. (A.60) and $a, b = 0, 1, 2$. The resulting system is given explicitly in [52, 37] and is of the form

$$\mathbf{A}^0 \partial_t \mathbf{u} + \mathbf{A}^i \partial_i \mathbf{u} + \mathbf{B}(\mathbf{u}, F) = 0, \tag{A.61}$$

where $F = (f, F^A, \partial_\mu f, \partial_\mu F^A)$ represents the gauge source functions and their derivatives. The matrices $\mathbf{A}^0, \mathbf{A}^i$ are symmetric and depend on the coordinate components of the frame. $\mathbf{A}^0$ is positive definite as long as $1-(e_1{}^0)^2-(e_2{}^0)^2-(e_3{}^0)^2 > 0$, which corresponds to e_0 being time-like. Characteristics are time-like and null.

The remaining components of Eqs. (A.50)–(A.52),

$$T_{ij}{}^\mu = 0, \quad \Delta_{ij}{}^L{}_K = 0, \quad H_{0k0} = 0, \quad \frac{1}{2} H_{jk0}\epsilon^{jk}{}_m = 0,$$

only contain derivatives in directions orthogonal to e_0 and are satisfied if satisfied initially by virtue of the evolution equations (see [52]). e_0 in general is not hypersurface orthogonal and therefore the constraints do contain derivatives in direction of ∂_t. In order to monitor these constraints during a numerical evolution, we eliminate the time derivatives by means of the evolution equations.

Appendix A.6.2. Numerical implementation The code is based on the Cactus Computational Toolkit [42] and the Kranc software [36, 37]. The spatial discretization of Eqs. (A.61) is done in a straight forward way

$$\partial_t \mathbf{u} = -(\mathbf{A}^0)^{-1}\mathbf{A}^i D_i \mathbf{u} + (\mathbf{A}^0)^{-1}\mathbf{B}(\mathbf{u}, F), \tag{A.62}$$

where D_i is the 2nd (or 4th order) accurate centered derivative operator in the direction i (see Appendix B.1). Time integration is done with the method of lines (CactusMoL) using ICN for the 2nd order scheme and RK4 for the 4th order scheme. If needed, artificial dissipation is added to the right hand side of equation (A.62) in the form

$$(\mathbf{A}^0)^{-1} Q_d \, \mathbf{u}, \tag{A.63}$$

where Q_d is the Kreiss-Oliger dissipation operator (see Appendix B.2). Respecting the symmetrizer in the dissipation term is essential, replacing it by the identity matrix triggered exponentially growing continuum modes e.g. for the gauge wave testbed with non-linear amplitude.

Appendix A.7. LSU_HyperGR

This symmetric hyperbolic first order formulation is described by Sarbach and Tiglio in [53]. The system has 34 evolved variables which are the standard ADM metric γ_{ij}, extrinsic curvature K_{ij} and lapse α, as well as extra variables $d_{kij} = \partial_k \gamma_{ij}$ and $A_i = \partial_i \alpha/\alpha$, introduced to make the formulation first order in space. In addition to the Hamiltonian constraint $\mathcal{H}$ and the momentum constraint $\mathcal{M}_i$, the constraints arising from those new variables are

$$C_{A_i} = A_i - \partial_i \alpha/\alpha, \tag{A.64}$$

$$C_{kij} = d_{kij} - \partial_k \gamma_{ij}, \tag{A.65}$$

$$C_{lkij} = \partial_{[l} d_{k]ij}. \tag{A.66}$$

The system of PDEs resulting from the standard ADM 3+1 decomposition of the Einstein equations is only weakly hyperbolic. To get a symmetric hyperbolic system the principal part has to be modified further. This is done by adding the constraints to the right hand sides of the evolution equations with appropriate multiplicative factors ζ, ξ, η, χ and ι. Here these parameters are chosen to be constant in space, although in general this is not necessary. The full set of equations is then

$$\partial_0 \gamma_{ij} = -2K_{ij}, \tag{A.67}$$

$$\partial_0 K_{ij} = R_{ij} - \frac{1}{\alpha}\nabla_i \nabla_j \alpha - 2K_{ia}K^a{}_j + K K_{ij} + \iota \gamma_{ij}\mathcal{H} + \zeta \gamma^{ab} C_{a(ij)b}, \tag{A.68}$$

$$\partial_0 d_{kij} = -2\partial_k K_{ij} - 2A_k K_{ij} + \eta \gamma_{k(i}\mathcal{M}_{j)} + \chi \gamma_{ij}\mathcal{M}_k, \tag{A.69}$$

$$\partial_0 \alpha = -F(\alpha, K, x^\mu) + S(x^\mu), \tag{A.70}$$

$$\partial_0 A_i = -\frac{\partial F(\alpha, K, x^\mu)}{\partial \alpha} A_i - \frac{1}{\alpha}\frac{\partial F(\alpha, K, x^\mu)}{\partial K}\partial_i K - \frac{1}{\alpha}\frac{\partial F(\alpha, K, x^\mu)}{\partial x^i} + \xi \mathcal{M}_i, \tag{A.71}$$

where $\partial_0 = (\partial_t - \mathcal{L}_\beta)/\alpha$, R_{ij} is the Ricci tensor and K the trace of the extrinsic curvature. The functions $F(\alpha, K, x^i)$ and $S(x^i)$ are pure gauge and can be chosen freely. The choices $S = 0$ and $F = \alpha K$ provides harmonic gauge conditions. Restriction of the parameters $\chi, \xi, \eta, \zeta, \iota$ to the family

$$\iota = -1/2, \ \zeta\eta = -2, \ \xi = -1/2\chi + 1/4\eta - 1/2 \tag{A.72}$$

results in a strongly hyperbolic system. A symmetric hyperbolic subfamily is given by $\zeta = -1$, which leaves χ as the single free parameter (constrained only by the condition $\chi \neq 0$). The runs presented here were done with the specific choice of $\chi = -1$.

To ensure a numerically stable discretization based on the energy method for hyperbolic equations, second order spatial differencing operators that satisfy the summation by parts (SBP) condition are used [54, 55]. Furthermore a small amount of dissipation (standard Kreiss-Oliger dissipation operators) is added to the right hand sides of the evolution equations. The integration in time is done with a third order Runge-Kutta scheme.

Appendix B. Numerical methods

Appendix B.1. Spatial discretization

Most of our numerical results are based on *second order accurate centered discretization*:

$$\partial_i \to D_{0i}\,, \qquad \partial_i\partial_j \to \begin{cases} D_{0i}D_{0j} & \text{if } i \neq j \\ D_{+i}D_{-i} & \text{if } i = j \end{cases}\,, \tag{B.1}$$

where

$$D_+ v_j := \frac{v_{j+1} - v_j}{\Delta x}, \tag{B.2}$$

$$D_- v_j := \frac{v_j - v_{j-1}}{\Delta x},$$

$$D_0 v_j := \frac{v_{j+1} - v_{j-1}}{2\Delta x},$$

$$D_+ D_- v_j := \frac{v_{j+1} - 2v_j + v_{j-1}}{\Delta x^2}. \tag{B.3}$$

For a summary of definitions and results for standard fourth order discretizations we again refer to [11], where in particular some results concerning the evolution systems considered here are derived.

Finally, averaging operators $A_\pm$ are defined as:

$$A_+ v_j := \frac{v_{j+1} + v_j}{2} \tag{B.4}$$

$$A_- v_j := \frac{v_j + v_{j-1}}{2}. \tag{B.5}$$

Appendix B.2. Artificial Dissipation

For second order accurate codes, it is common practice to add third order accurate Kreiss–Oliger dissipation [56] to all right-hand-sides of the time evolution equations as

$$\partial_t \mathbf{u} \to \partial_t \mathbf{u} + Q\mathbf{u}. \tag{B.6}$$

Here we use the following general form of the Kreiss–Oliger dissipation operator Q of order $2r$,

$$Q = \sigma(-h)^{2r-1}(D_+)^r \rho (D_-)^r / 2^{2r}, \tag{B.7}$$

for a $2r-2$ accurate scheme, where the parameter σ regulates the strength of the dissipation and ρ is a weighting function, which is typically set to 1 in the interior but

may go to 0 at the boundary. Since we mostly focus on second order accurate codes here, the relevant case is $r = 2$, for which

$$Q = -\sigma h^3 (D_+)^2 \rho (D_-)^2 / 16, \tag{B.8}$$

which may be implemented using Erik Schnetter's Cactus thorn `AEIThorns/Dissipation` [21].

References

[1] Susan G. Hahn and Richard W. Lindquist. The two body problem in geometrodynamics. *Ann. Phys.*, 29:304–331, 1964.

[2] Frans Pretorius. Evolution of binary black hole spacetimes. *Phys. Rev. Lett.*, 95:121101, 2005.

[3] Manuela Campanelli, Carlos O. Lousto, Pedro Marronetti, and Yosef Zlochower. Accurate evolutions of orbiting black-hole binaries without excision. *Phys. Rev. Lett.*, 96:111101, 2006.

[4] John G. Baker, Joan Centrella, Dae-Il Choi, Michael Koppitz, and James van Meter. Gravitational wave extraction from an inspiraling configuration of merging black holes. *Phys. Rev. Lett.*, 96:111102, 2006.

[5] Apples With Apples: Numerical Relativity Comparisons and Tests: `http://www.ApplesWithApples.org`.

[6] Miguel Alcubierre, Gabrielle Allen, Thomas W. Baumgarte, Carles Bona, David Fiske, Tom Goodale, Francisco Siddhartha Guzmán, Ian Hawke, Scott Hawley, Sascha Husa, Michael Koppitz, Christiane Lechner, Lee Lindblom, Denis Pollney, David Rideout, Marcelo Salgado, Erik Schnetter, Edward Seidel, Hisa aki Shinkai, Deirdre Shoemaker, Béla Szilágyi, Ryoji Takahashi, and Jeffrey Winicour. Towards standard testbeds for numerical relativity. *Class. Quantum Grav.*, 21(2):589–613, 2004.

[7] Horst Beyer and Olivier Sarbach. On the well posedness of the Baumgarte-Shapiro- Shibata-Nakamura formulation of Einstein's field equations. *Phys. Rev. D*, 70:104004, 2004.

[8] C. Gundlach and J.M. Martin-Garcia. Symmetric hyperbolic form of systems of second-order evolution equations subject to constraints. *Phys. Rev. D*, 70:044031, 2004.

[9] Carsten Gundlach and Jose M. Martin-Garcia. Symmetric hyperbolicity and consistent boundary conditions for second-order Einstein equations. *Phys. Rev. D*, 70:044032, 2004.

[10] Carsten Gundlach and Jose M. Martin-Garcia. Hyperbolicity of second-order in space systems of evolution equations. *Class. Quantum Grav.*, 23:S387–S404, 2006.

[11] Gioel Calabrese, Ian Hinder, and Sascha Husa. Numerical stability for finite difference approximations of Einstein's equations. *J. Comp. Phys.*, 218:607–634, 2006.

[12] B. Szilágyi, H-O. Kreiss, and J. Winicour. Modeling the black hole excision problem. *Phys. Rev. D*, 71:104035, 2005.

[13] Mohammad Motamed, M. C. Babiuc, B. Szilagyi, H-O. Kreiss, and J.Winicour. Finite difference schemes for second order systems describing black holes. *Phys. Rev. D*, 73:124008, 2006.

[14] *Computational Fluid Dynamics Wiki / Validation and test cases*, CFD Online, `http://www.cfd-online.com/Wiki/Validation_and_test_cases`.

[15] Test set for IVP solvers. `http://pitagora.dm.uniba.it/~testset/`.

[16] R. Courant and K. O. Friedrichs. *Supersonic flows and shock waves*. Springer, Berlin, 1976.

[17] G. Nagy, O. E. Ortiz, and O. A. Reula. Strongly hyperbolic second order Einstein's evolution equations. *Phys. Rev. D*, 70:044012, 2004.

[18] Carsten Gundlach and Jose M. Martin-Garcia. Well-posedness of formulations of the Einstein equations with dynamical lapse and shift conditions. *Phys. Rev. D*, 74:024016, 2006.

[19] G. Calabrese, J. Pullin, O. Sarbach, and M. Tiglio. Convergence and stability in numerical relativity. *Phys. Rev. D*, 66:041501, 2002.

[20] Bertil Gustafsson, Heinz-Otto Kreiss, and Joseph Oliger. *Time dependent problems and difference methods*. Wiley, New York, 1995.

[21] Erik Schnetter. `AEIThorns/Dissipation` Cactus thorn.

[22] Maria C. Babiuc, Béla Szilágyi, and J. Winicour. Some mathematical problems in numerical relativity. *Lect. Notes Phys.*, 692:251–274, 2006.

[23] Sascha Husa, Carsten Schneemann, Tilman Vogel, and Anil Zenginoglu. Hyperboloidal data and evolution. 2005. To appear in Proceedings of the 2005 spanish relativity meeting, AIP Conference Proceedings, 8 pages.

[24] Maria C. Babiuc, Béla Szilágyi, and Jeffrey Winicour. Testing numerical relativity with the shifted gauge wave. *Class. Quantum Grav.*, 23:S319–S342, 2006.

[25] Maria C. Babiuc, Béla Szilágyi, and J.Winicour. Harmonic initial-boundary evolution in general relativity. *Phys. Rev. D*, 73:064017, 2006.
[26] R. H. Gowdy. *Phys. Rev. Lett.*, 27:826, 1971.
[27] H. Ringstrom. On a wave map equation arising in general relativity. 2003.
[28] Kimberly C. B. New, Keith Watt, Charles W. Misner, and Joan M. Centrella. Stable 3-level leapfrog integration in numerical relativity. *Phys. Rev. D*, 58:064022, 1998. gr-qc/9801110.
[29] Jorg Frauendiener and Tilman Vogel. Algebraic stability analysis of constraint propagation. *Class. Quantum Grav.*, 22:1769–1793, 2005.
[30] Sascha Husa. In L. Fernández and L. Manuel González, editors, *Current trends in relativistic astrophysics*, volume 617 of *Lecture Notes in Physics*. Springer, 2002.
[31] B.K. Berger. Asymptotic behavior of a class of expanding gowdy spacetimes. *submitted to Phys. Rev. D*, 2002.
[32] David Garfinkle. Harmonic coordinate method for simulating generic singularities. *Phys. Rev. D*, 65:044029, 2002.
[33] D. E. Post and L. G. Votta. Computational science demands a new paradigm. *Physics Today.*, 58:35, 2005.
[34] M. Boyle, L. Lindblom, H. Pfeiffer, M. Scheel, and L. Kidder. Testing the accuracy and stability of spectral methods in numerical relativity. *Phys. Rev.*, D75:024006–024018, 2007.
[35] Oliver Rinne. Stable radiation-controlling boundary conditions for the generalized harmonic einstein equations. *Class. Quantum Grav.*, 23:6275–6300, 2006.
[36] Sascha Husa, Ian Hinder, and Christiane Lechner. Kranc: a Mathematica application to generate numerical codes for tensorial evolution equations. *Comput. Phys. Comm.*, 174:983–1004, 2006.
[37] D. Alic. Toward the numerical implementation of well-posed, constraint preserving evolution systems for general relativity. Master's thesis, University of Timisoara, 2005.
[38] Ian Hinder. *Well-posed formulations and stable finite differencing schemes for numerical relativity*. PhD thesis, University of Southampton, Southampton, UK, 2005.
[39] Richard Arnowitt, Stanley Deser, and Charles W. Misner. The dynamics of general relativity. In L. Witten, editor, *Gravitation: An introduction to current research*, pages 227–265. John Wiley, New York, 1962.
[40] James W. York. Kinematics and dynamics of general relativity. In Larry L. Smarr, editor, *Sources of gravitational radiation*, pages 83–126. Cambridge University Press, Cambridge, UK, 1979.
[41] Simonetta Frittelli. Note on the propagation of the constraints in standard 3+1 general relativity. *Phys. Rev. D*, 55:5992–5996, 1997.
[42] Cactus Computational Toolkit. `http://www.cactuscode.org`.
[43] B. Szilágyi and Jeffrey Winicour. Well-posed initial-boundary evolution in general relativity. *Phys. Rev. D*, 68:041501, 2003.
[44] Takashi Nakamura, Ken-ichi Oohara, and Yasufumi Kojima. General relativistic collapse to black holes and gravitational waves from black holes. *Prog. Theor. Phys. Suppl.*, 90:1–218, 1987.
[45] Takashi Nakamura and Ken-ichi Oohara. Methods in 3D numerical relativity. In C. Evans, L. Finn, and D. Hobill, editors, *Frontiers in Numerical Relativity*, pages 254–280. Cambridge University Press, Cambridge, England, 1989.
[46] Masaru Shibata and Takashi Nakamura. Evolution of three-dimensional gravitational waves: Harmonic slicing case. *Phys. Rev. D*, 52:5428, 1995.
[47] Thomas W. Baumgarte and Stuart L. Shapiro. On the numerical integration of Einstein's field equations. *Phys. Rev. D*, 59:024007, 1999.
[48] Miguel Alcubierre, Bernd Brügmann, Thomas Dramlitsch, José A. Font, Philippos Papadopoulos, Edward Seidel, Nikolaos Stergioulas, and Ryoji Takahashi. Towards a stable numerical evolution of strongly gravitating systems in general relativity: The conformal treatments. *Phys. Rev. D*, 62:044034, 2000.
[49] Miguel Alcubierre, Bernd Brügmann, Peter Diener, Michael Koppitz, Denis Pollney, Edward Seidel, and Ryoji Takahashi. Gauge conditions for long-term numerical black hole evolutions without excision. *Phys. Rev. D*, 67:084023, 2003.
[50] Sascha Husa. The FlexBSSN code is available on request from the author.
[51] Y. Zlochower, J. G. Baker, M. Campanelli, and C. O. Lousto. Accurate black hole evolutions by fourth-order numerical relativity. *Phys. Rev. D*, 72:024021, 2005.
[52] Helmut Friedrich and Gabriel Nagy. The initial boundary value problem for Einstein's vacuum field equations. *Commun. Math. Phys.*, 201:619–655, 1999.
[53] O. Sarbach and M. Tiglio. Exploiting gauge and constraint freedom in hyperbolic formulations

of Einstein's equations. *Phys. Rev. D*, 66:064023, 2002.

[54] B. Strand. Summation by parts for finite differencing approximations for d/dx. *J. Comput. Phys.*, 110:47, 1994.

[55] Luis Lehner, Oscar Reula, and Manuel Tiglio. Multi-block simulations in general relativity: high order discretizations, numerical stability, and applications. *Class. Quantum Grav.*, 22:5283–5322, 2005.

[56] Heinz Otto Kreiss and Joseph Oliger. *Methods for the approximate solution of time dependent problems*. GARP publication series No. 10, Geneva, 1973.